Studies on colloidal and emulsifying properties of naturally-derived molecular assemblies

Toya Ishii

2019

CONTENTS

GENERAL INTRODUCTION

A wide variety of food products containing oil and water, e.g., dressings, sauces, creams, beverages, etc. are defined as oil-in-water (O/W) emulsions, where oil is dispersed as small colloidal oil droplets in an aqueous continuous phase (McClements, 2016). O/W emulsions are usually produced by homogenizing oil and water with surface-active amphiphilic molecules such as synthesized low-molecular-weight surfactants and natural proteins, which act as emulsifying agents, that is, adsorb newly-created oil-water interfaces and form interfacial adsorbed layers to stabilize oil droplets.

Since the interface between incompatible oil and water is thermodynamically unstable, i.e., energy level at the interface is high (Walstra, 2003; McClements, 2016), O/W emulsions containing a large area of the oil-water interfaces covered by emulsifying agents are generally thermodynamically metastable systems (i.e., kinetically stable states) (McClements, 2016). The dispersed oil droplets once emulsified inevitably undergo undesirable physical phenomena such as creaming, flocculation, and coalescence to separate into bulk oil and water (McClements, 2016). These physical phenomena normally impair product quality such as appearance and texture; therefore, controlling and delaying the progress of these destabilization phenomena for appropriate periods before consumption are critically important for the design and development of food emulsion products.

The kinetic stability of O/W emulsions is determined to a great extent by characteristics of emulsifying agents covering emulsion oil droplet surfaces. While low-molecular-weight surfactants effectively prevent droplet coalescence by the Gibbs-Marangoni effect (McClements, 2016), proteins can stabilize oil droplets by adsorbing to oil-water interfaces and form viscoelastic protective layers on the oil droplet surfaces

(McClements, 2016). In food industries, proteins originated from milk and egg are mainly applied to many emulsified foods as indispensable emulsifying agents due to their outstanding ability to stabilize emulsified oil droplets. Actually the emulsifying properties of these animal-based proteins are almost satisfactory for achieving the formation of kinetically stable emulsions. However, since the production of animal-based materials needs much more energy compared to that of materials from other resources, e.g., plant and microbials (Pimentel & Pimentel, 2003; Tuomisto, 2018), the emulsifying agents from other eco-friendly resources that can be counterparts of animal proteins are increasingly required from now on in order to ensure food security. In addition to this aspect, consumers' requirements for food products are nowadays increasing and diversifying, e.g., natural, health-beneficial, religiously-acceptable, less allergenic, etc. Although it is difficult to develop the emulsifying agent that can both displace milk and egg proteins functionally and meet all such requirements of consumers perfectly, novel natural and eco-friendly emulsifying agents ought to be explored to increase the additional practical options that can appropriately satisfy the consumers' demands.

To find clues for the possible candidates from other edible resources, the author of this work sought a hint in the examples of a conventional animal-based emulsifying agent and synthesized inedible materials studied in the polymer science field. Egg yolk is one of the most-widely used edible animal-based emulsifying agents due to the ability to form physically-stable emulsions (Hatta, Hagi, & Hirano, 1997). The emulsifying ability of egg yolk is attributed to the major egg yolk component called low density lipoprotein (LDL), a submicron globules formed by assembling neutral lipid, polar lipid, and lipophilic protein molecules to enable hydrophobic neutral lipids well-dispersed in an aqueous media (Mine, 1998; Martinet, Saulnier, Beaumal, Courthaudon, & Anton, 2003; Jolivet, Boulard, Beaumal, Chardot, & Anton, 2006). The author recognized that similar submicron complexes of protein

and lipid molecules called oil bodies/oleosomes exist in tissues of oil-producing plants like soybean (Huang, 1992), and conceived the idea that plant oil bodies can act as an emulsifying agent like egg yolk. On the other hand, in the area of polymer science, several research groups recently reported assembly of synthesized surface-active macromolecules into colloidal particles for creating the new type of emulsifying agents that can achieve enhanced emulsion stability, stimuli responsibility, etc. (Ngai, Behrens, & Auweter, 2005; Schmidt, Liu, Rütten, Phan, Möller, & Richtering, 2011), implying that application of molecular assemblies based on edible biopolymers as emulsifying agents can be a promising approach to establishing unconventional food emulsion systems.

In this context, the author studies the possibility of naturally-derived molecular assemblies as a novel class of edible emulsifying agents in this thesis. As molecular assemblies naturally existing in plant resources, the author deals with soybean seed oil bodies. Depending on aqueous extraction conditions from soybean seeds, the composition of proteins involved in oil bodies varies as shown in previous studies (Iwanaga, Gray, Fisk, & Decker, 2007; Chen & Ono, 2010; Fisk & Gray, 2011). Soybean oil bodies extracted at neutral pH accompany soybean seed storage proteins, e.g., glycinin and β-conglycinin on the oil body surfaces, whereas oil bodies extracted at pH 11 hardly include such exogeneous proteins on the surface (Chen & Ono, 2010). The author carried out oil body extraction under both the two conditions to obtain the two types of oil bodies, respectively, and compared their colloidal and emulsifying properties (Chapter 1).

Commercial food emulsion products mostly include various solutes such as acids and salts that modify the aqueous conditions, e.g., pH values and ion strength (Hunter, 2001). These aqueous condition changes generally influence colloidal and emulsifying properties of dispersed particles (McClements, 2016). Towards practical application, the author clarifies the

effects of acid and salt addition on colloidal and emulsifying properties of purified soybean oil bodies extracted at pH 11 (Chapter 2).

Although proteins are the most widely-used natural emulsifying agents due to their amphiphilic nature, protein ingestion is occasionally avoided or reduced by some consumers who have an allergy to particular proteins or are suffering from kidney disease. Therefore, non-proteinous emulsifying agents from natural and eco-friendly origins are in demand. Using natural food-grade gelling polysaccharides originated from plant and microbials, the author fabricates molecular-assembling microgels and tries to prepare polysaccharide microgel-based emulsions (Chapter 3).

References

Chen, Y. & Ono, T. (2010). Simple Extraction Method of Non-allergenic Intact Soybean Oil Bodies That Are Thermally Stable in an Aqueous Medium. Journal of Agricultural and Food Chemistry, 58 (12), 7402–7407.

Fisk, I. D. & Gray, D. A. (2011). Soybean (Glycine max) Oil Bodies and Their Associated Phytochemicals. Journal of Food Science, 76 (9), 1349–1354.

Hatta, H., Hagi, T., & Hirano, K. (1997) Hen Eggs: their basic and applied science (eds Ymamoto, T., Juneja, L. R., Hatta, H., & Kim, M.) Ch. 8. CRC Press.

Huang, A. H. C. (1992). Oil Bodies and Oleosins in Seeds. Annual Review of Plant Physiology and Plant Molecular Biology, 43 (1), 177–200.

Hunter, R. J. (2001) Foundations of Colloid Science 2nd edn. Oxford University Press.

Iwanaga, D., Gray, D. A., Fisk, I. D., Decker, E. A., Weiss, J., & McClements, D. J. (2007). Extraction and characterization of oil bodies from soy beans: A natural source of pre-emulsified soybean oil. Journal of Agricultural and Food Chemistry, 55 (21), 8711–8716.

Jolivet, P., Boulard, C., Beaumal, V., Chardot, T., & Anton, M. (2006). Protein components of low-density lipoproteins purified from hen egg yolk. Journal of Agricultural and Food Chemistry, 54 (12), 4424–4429.

Kiosseoglou, V. & Sherman, P. (1983). Influence of egg yolk lipoproteins on the rheology and stability of oil/water emulsions and mayonnaise 1. Viscoelasticity of groundnut oil-in-water emulsions and mayonnaise. Journal of Texture Studies, 14 (4), 397–417.

Martinet, V., Saulnier, P., Beaumal, V., Courthaudon, J. L., & Anton, M. (2003). Surface properties of hen egg yolk low-density lipoproteins spread at the air–water interface. Colloids and Surfaces B: Biointerfaces, 31 (1-4), 185–194.

McClements, D. J. (20016) Food Emulsions: principles, practices, and techniques 3rd edn. CRC Press.

Mine, Y. (1998). Adsorption Behavior of Egg Yolk Low-Density Lipoproteins in Oil-in-Water Emulsions. Journal of Agricultural and Food Chemistry, 46 (1), 36–41.

Ngai, T., Behrens, S. H., & Auweter, H. (2005) Novel emulsions stabilized by pH and temperature sensitive microgels. Chem. Commun. 41, 331–333.

Pimentel, D. & Pimentel, M. (2003) Sustainability of meat-based and plant-based diets and the environment. *Am. J. Clin. Nutr.* **78** (Suppl), 660S–663S.

Schmidt, S, Liu, T., Rütten, S., Phan, K. H., Möller, M., & Richtering, W. (2011) Influence of microgel architecture and oil polarity on stabilization of emulsions by stimuli-sensitive core–Shell poly(N-isopropylacrylamide-co-methacrylic acid) microgels: Mickering versus Pickering behavior? Langmuir 27, 9801–9806.

Tuomisto, H. L. (2018). The eco-friendly burger—Could cultured meat improve the environmental sustainability of meat products? EMBO reports, 20, e47395.

Walstra, P. (2003) Physical Chemistry of Foods. Marcel Dekker Inc., 2003

Chapter 1:
Interfacial and emulsifying properties of crude and purified soybean oil bodies

1. Introduction

Many food products such as ice creams, dressings, and mayonnaises exist as an oil-in-water (O/W) emulsion where an oil phase is dispersed in a continuous aqueous phase. The emulsion system is usually stabilized by synthesized low-molecular-weight emulsifiers often in combination with natural resources, whereas consumers nowadays tend to avoid the emulsifiers because of an increasing demand for natural materials. High-molecular-weight functional animal proteins like milk proteins are widely used in the food industry, while such animal proteins often need more energy for the production, compared to that of plant materials (Pimentel & Pimentel, 2003; Pimentel et al., 2008). Plant materials also attract the consumers' attention due to their health benefits based on various secondary metabolites. Natural and environment-friendly emulsifying agents from plant resources are highly required as a substitute for functional animal proteins (Rodrigues, Coelho, & Carvalho, 2012; Karaca, Low, & Nickerson, 2015; McClements & Gumus, 2016).

Since the energy cost of soybean production is relatively lower than other crops mainly based on their high nitrogen fixation ability (Liu, 1997), soybean proteins as a natural-based emulsifying agent are enthusiastically investigated in the previous researches (Palazolo, Mitidieri, & Wagner, 2003; Palazolo, Sorgentini, & Wagner, 2005; Keerati-u-rai & Corredig, 2009; Palazolo, Sobral, & Wagner, 2011). Soybean proteins are usually isolated from defatted soybeans in the food industry and mainly consist of storage proteins, e.g. β-conglycinin (7S) and glycinin (11S). They are hydrophilic globular proteins that have good emulsifying

properties (Chove, Grandison, & Lewis, 2001; Keerati-U-Rai & Corredig, 2010; Molina, Papadopoulou, & Ledward, 2001), but the properties are not necessarily better than those of animal proteins (Hu, McClements, & Decker, 2003; Amine, Dreher, Helgason, & Tadros, 2014). In this context, recently, there have been an increasing interest in lipophilic membrane proteins called oleosin, another component of soybean seeds that can be also seen in various crop seeds (Rayner, 2015). Oleosins are composed of hydrophilic and hydrophobic domains (Huang, 1992), related to the surface activity at the air-water (A/W) or oil-water (O/W) interface. Nikiforidis et al. (2013) indicated that the purified oleosins from maize form strong elastic films at the A/W interface. Wijesundera et al. (2013) and Deleu et al. (2010) reported that oleosins from canola and rapeseed can stabilize O/W emulsions for several weeks. On the other hand, even though Samoto et al. (2007) successfully collected an oleosin-rich fraction from defatted soybean meals, almost pure oleosin fractions cannot be easily isolated from the meals due to strong tendency of hydrophobic oleosins to form aggregates without covering oil droplets and due to abundance of other seed proteins such as 7S and 11S. This situation is different from the other crops such as maize, sesame, and ripe seed.

Soybean oleosins are originally present in an intracellular organelle, so-called oil body, oleosome or lipid body depending on the literature. They are known to cover neutral lipids globules containing phytosterols and tocopherols together with phospholipids (Tzen & Huang, 1992; Fisk & Gray, 2011; Chen, Cao, Zhao, Kong, & Hua, 2014). The hydrophobic domain of oleosins is embedded into the lipids globules across the phospholipids monolayer, while the hydrophilic domains cover the surface of the lipids globules (Tzen & Huang, 1992; Huang, 1992). Since the oleosins and phospholipids form a strong membrane, oil bodies are stable against coalescence and lipid oxidation during seed dehydration (Huang, 1992); therefore, several researchers expected oil bodies from sunflower seed, maize germ, and soybean seed as

pre-emulsified capsules carrying hydrophobic bioactive materials (White et al., 2008; Nikiforidis & Kiosseoglou, 2009; Chen, McClements, Gray, & Decker, 2012; Wu et al., 2012; Wu et al., 2011)). In these researches, oil bodies are often extracted from soybean seeds via an aqueous extraction, in which soybeans soaked in water are homogenized by a high speed mixer (Chen et al., 2012). During the homogenization process, oil bodies inevitably involve other seed proteins, i.e., 7S, 11S, allergen proteins (Gly m Bd 30 k etc.), and trypsin inhibitor (Chen & Ono, 2010). Recently Chen & Ono (2010) reported that these involved proteins can be removed from oil bodies under alkaline conditions to prepare intact oil bodies.

Several researches have been carried out to characterize interfacial properties of intact oil bodies. The intact oil bodies extracted under the alkaline condition above pH 9.0 adsorb to the A/W interface and seem to rupture and spread onto the interface (Maurer et al., 2013; Waschatko, Junghans, & Vilgis, 2012 (a)). Waschatko also reported in another study that purified oil bodies adsorbed to the A/W interface to form elastic films (Waschatko, Schiedt, Vilgis, & Junghans (2012 (b)). Maurer et al. (2013) investigated fundamental roles of soybean oleosin for stabilizing oil bodies and directly compared O/W emulsions stabilized by the intact and enzymatically-modified oil bodies to prove the function of oleosins themselves. These results imply that isolated and non-modified oil bodies play an important role in stabilizing the interfaces. In fact, egg yolk low density lipoproteins (LDL) as a complex globule structured by neutral lipids, phospholipids, and lipophilic proteins are considered to be responsible for emulsifying ability of egg yolk (Kiosseoglou & Sherman, 1983), probably due to its complex structure to allow the lipophilic proteins to easily access the O/W interface without possible aggregation (Mine, 1998; Martinet, Saulnier, Beaumal, Courthaudon, & Anton, 2003; Jolivet, Boulard, Beaumal, Chardot, & Anton, 2006). Considering practical use of the intact oil bodies in the food industry, however, sufficient fundamental information of the intact oil bodies such

as interfacial properties at the O/W interface and emulsifying properties are still unavailable.

The objective of this study is to reveal interfacial and emulsifying properties of the intact oil bodies (OB) from soybeans via the aqueous extraction under a condition of pH 11.0 in comparison with crude oil bodies that involve the other proteins (OBC) prepared in the more simplified way without pH adjustments. Colloidal and structural properties of OB and OBC were analyzed by particle size and zeta-potential measurements, SDS-PAGE, and pendant drop tensiometry. Subsequently, emulsifying properties of OB and OBC were evaluated by particle size measurement, visual observation, microscopy, and compositional analysis of oil droplet surfaces.

2. Materials & Methods

2.1. Materials

Commercial dried soybeans (*Glycine max* (L.) Merr. 'Tamahomare') for OB and OBC extraction were purchased from local market. Soybean oil, sucrose, and sodium dodecyl sulphate (SDS) were purchased from Wako Pure Chemical Industries Ltd., Japan. Precast polyacrylamide gel (e-PAGEL mini gel E-T1020L, 10-20%) was bought from ATTO CO., LTD., Japan. Florisil was purchased from Sigma Aldrich, USA. BCA protein assay kit was bought from Takara Bio Inc., Japan. Deionized water was used for preparation of all reagents and samples.

2.2. Preparation of OBC and OB suspensions

2.2.1. Extraction of OBC and OB

OB and OBC were extracted according to Chen & Ono (2010). Soybeans (50 g) were soaked overnight in deionized water at 4°C, and then the excessive unabsorbed water was discarded. The remained soaked soybeans were rinsed twice with deionized water, and subsequently ground with 200 ml of additional deionized water in a mixer (BM-RE08, Zojirushi Co., Japan) for 1 min. The homogenate was filtrated through three layers of gauze to obtain approximately 200 g of raw soymilk, followed by the addition of sucrose to achieve a final concentration of 20 wt%.

For OBC preparation, the mixture was centrifuged using a centrifuge (Kubota 3740, Kubota Co., Japan) at 4°C for 40 min at 22,140*g*. The top cream layer was collected and dispersed into another 70 ml of 20 wt% sucrose solution, and then the dispersion was centrifuged at the same condition described above; this washing process was repeated again. For OB preparation, the pH value of raw soymilk containing 20 wt% of sucrose was adjusted to

11.0 with 1 M NaOH, followed by centrifugation under the same condition stated above. Except for adjusting the pH value of sucrose solution to 11.0, the top layer was collected and washed in the same way as OBC preparation.

In order to remove sucrose, the OB and OBC were dispersed into 70 ml of 10 mM sodium phosphate buffer solution (pH 7.0). Subsequently, these dispersions were centrifuged under the same condition described above, and then the top layer was collected and dispersed into another phosphate buffer solution. Finally, the OB and OBC were collected from the dispersion via the centrifugation and mixed with 40 ml of phosphate buffer solution again. The mixtures were stirred on a magnetic stirrer overnight to ensure the complete dispersion. These dispersions were stored at 4°C with 0.02% (w/v) of sodium azide as an antimicrobial agent.

2.2.2. Standardization of the concentration of OB and OBC dispersion

In order to standardize the concentration of OB and OBC, a small aliquot (3 ml) of OB and OBC dispersion was poured into an aluminum cup to measure the total weight of the samples, and then heat-dried at 130°C for 3 h (AOAC Method 925.10) to measure the dry weight (Kapchie, Towa, Hauck, & Murphy, 2010). Based on the results, the solid content of original OB and OBC dispersion was determined, and OB and OBC were appropriately diluted with 10 mM sodium phosphate buffer (pH 7.0) to obtain 1 wt% of OB or OBC suspension.

2.3. Particle size measurement

Particle size distribution of OB, OBC, and corresponding emulsions (OB-E and OBC-E, described in the section 2.9) were analyzed by a laser diffraction particle size analyzer (SALD 2200, Shimadzu Co., Japan). Each sample was dispersed to the phosphate buffer and measured at 25°C; a refractive index of 1.45 was used for calculation of particle size distribution.

2.4. Microstructure observation of OB and OBC

The microstructure of both OB and OBC was observed using a scanning transmission electron microscope (STEM) (SU8230, Hitachi, Japan) with the BF-STEM detector by negative staining method. A 150 or 200 mesh cupper grid covered with a polyvinyl formal film with carbon coating was hydrophilized and used for sampling. Both 0.1 wt% of OB and OBC in 10 mM phosphate buffer solution (pH 7.0) was placed on the grid, and then stained with phosphotungstic acid, respectively. These samples were observed with the acceleration voltage of 30 kV.

2.5. Protein analysis of OB and OBC

2.5.1. Quantification of protein content

The protein content of OB and OBC was quantified by the BCA method using Takara BCA protein assay kit (Takara Bio Inc., Japan). After freeze drying of 5 ml of OB and OBC dispersions, the residues were mixed with 30 ml of 4% (w/v) SDS solution on a vortex mixer and the mixtures were stored overnight at room temperature to extract proteins. Then they were subsequently centrifuged for 30 min at 22,140*g* to separate the slurry into an aqueous phase and an oil phase. An aliquot (10 μl) of the aqueous phase was used for protein assay, respectively.

2.5.2. SDS-PAGE

SDS-PAGE was carried out according to Laemmli (1970) to analyze the protein composition of OB and OBC using 10-20% gradient gel. Each suspension containing 1 wt% of either OB or OBC was mixed with an equal amount of 2× sample buffer containing 0.5 M Tris-HCl (pH6.8), 4%(w/v) SDS, 20%(w/v) glycerol, and 0.2 (w/v) BPB, and then 2-melcapto ethanol was added

to the mixture up to 5% (v/v). After an incubation for 2 hours at 40°C, the samples were loaded into the gel and electrophoresed at 100 V followed by a CBB staining.

2.6. Zeta-potential measurement

Zeta-potential of OB and OBC was measured using a laser-Doppler zeta-potential analyzer (ELS-Z1, Otsuka Electronics Co. Ltd., Japan). To avoid multiple scattering, OB and OBC were diluted with the phosphate buffer to a desired concentration (approximately 2500 times). Measurements were performed at 25°C.

2.7. Interfacial properties measurements of OB and OBC at the O/W interface

2.7.1. Purification of soybean oil

Polar components such as fatty acids and di- or mono- acylglycerols were removed from soybean oil to avoid their influence in the following experiments. Florisil was added to soybean oil to a final concentration of 4 wt%, followed by stirring on a magnetic stirrer for 30 min at room temperature (Murphy, Farkas, & Jones, 2016). The mixture was centrifuged for 30 min at 22,140×g to precipitate Florisil from oil fraction absolutely. The obtained purified soybean oil was stored in a shade bottle at room temperature.

2.7.2. Interfacial tension and dilatational viscoelasticity measurements

Interfacial tension and dilatational viscoelasticity at the O/W interface were analyzed for OB and OBC suspensions by the Pendant drop method using a tensiometer (Tracker, Teclis, France). A needle tip of micro cylinder filled with sample suspension was immersed into the purified soybean oil. A droplet of the suspension was formed into the oil phase via the needle tip and the interfacial area of the droplet was controlled and oscillated sinusoidally. The initial interfacial

area was 30 mm^2 and the oscillation amplitude was 3 mm^2. One cycle was set up 20 sec, and 2 active cycles and 13 blank cycles were repeated for 7200 sec at 25°C.

Before sample measurements, interfacial tension between the purified soybean oil and 10 mM phosphate buffer solution (pH 7.0) was measured as blank measurements to check the purity of these two phases. After sample measurements, time-dependent change of their interfacial tension, storage modulus (E'), and loss modulus (E") were analyzed. Loss tangent (tanδ, E"/E') were calculated and plotted as a function of interfacial pressure which was defined as the difference between interfacial tension $_{sample/oil}$ and interfacial tension $_{blank}$.

2.8. Emulsion preparation

The purified soybean oil was added to 1 wt% OB or OBC suspension to achieve a final concentration of 10 wt%. They were emulsified by a high speed blender (Physcotron, Microtec, Japan) with NS-20 shaft at 15,000 rpm for 3 min to prepare OB-stabilized emulsion (OB-E) and OBC-stabilized emulsion (OBC-E), respectively.

2.9. Stability test

After emulsification, OB-E and OBC-E were characterized using the particle size analyzer (described in 2.4.). OB-E and OBC-E containing sodium azide (0.02% (w/v)) as an antimicrobial agent were stored in glass vials for 14 days at room temperature to evaluate oil phase separation, aggregation, and coalescence. They were subjected to visual observation and particle size analysis in which the samples were gently mixed to ensure homogeneity. The stability of these emulsions against aggregation and coalescence was evaluated depending on a relative particle size change, a dimensionless parameter calculated from the following equation:

$$\text{Relative particle size change} = \frac{d_{4,3}}{d_{4,3}\ (\text{day } 0)}$$

, where $d_{4,3}$ is the volume-weighted particle size calculated from a large peak (> 1.57 μm) of each particle size distribution.

2.10. Characterization of proteins adsorbed onto the emulsion droplet surface

To characterize adsorbed proteins of OB-E and OBC-E, the emulsions (25 ml) were centrifuged at 100*g* for 5 min to separate them into an opaque layer rich in oil droplets and a clear serum layer. The clear layer was removed carefully with a syringe. The left opaque layer was redispersed into another 20 ml of phosphate buffer solution and then centrifuged under the same condition described before. This fractionating process was carried out again to collect emulsion oil droplets without non-adsorbed materials. The droplets covered by adsorbed materials were freeze-dried and defatted three times using 10 ml of acetone coupled with centrifugations (22140×g, 4°C, 5 min) and solvent removals. The obtained adsorbed materials were dissolved into 2 wt% SDS solution to determine the protein content and composition via the BCA method and SDS-PAGE (described in 2.5), respectively. The surface protein load was calculated as reported by McClements (1999).

2.11. Microstructure observation of OB-E and OBC-E

OB-E and OBC-E were observed using a scanning electron microscope (SEM) (SU8230, Hitachi, Japan) with the LA-BSE detector equipped with a Cryo-unit (Alto2500, Gatan UK, UK). A tiny metal tube including an aliquot of sample emulsions was rapidly frozen in slush nitrogen, and then cleaved and sublimated. The cleaved surface was coated with platinum using an ion spatter and observed with 10 kV of acceleration voltage.

2.12. Statistical analysis

All experiments were repeated at least three times. Typical image or graph was shown as a result of SDS-PAGE, particle size analysis, and microscopy. The other results were represented by mean ± standard deviation.

3. Results & Discussion

3.1. Fundamental properties of OB and OBC

3.1.1 Droplet profiles

To clarify the dispersibility of OB and OBC, particle size analysis was conducted using a laser diffraction particle size analyzer. Fig. 1-1 shows the particle size distribution and the volume weighted average particle size ($d_{4,3}$) of OB and OBC extracted from soybeans via the centrifugation and pH adjustment. The particle size of OB was almost smaller than 1 μm ($d_{4,3}$ = 0.59 ± 0.03 μm), while droplets larger than 1μm were found in the OBC dispersion ($d_{4,3}$ = 0.70 ± 0.08 μm) probably due to aggregates formed during the repeated centrifugations, suggesting that OBC are more susceptible to aggregation. Previous researches reported that the size of oil bodies was within the range approximately from 0.1 to 1.0 μm (Chen & Ono, 2010; Iwanaga et al., 2007). The obtained data correspond to the previous researches, indicating that OB and OBC are successfully collected by this method.

To understand the mechanisms where OB and OBC were susceptible to aggregation during the extraction stage, the zeta-potential of OB and OBC was measured using a laser-Doppler zeta-potential analyzer to estimate the electrostatic repulsion between particles in the OB and OBC dispersion. The zeta-potential of OB and OBC was -14.2 ± 1.9 mV and -39.0 ± 4.1 mV, respectively, indicating that there was a stronger electrostatic repulsion between OBC than that between OB. The potential of OBC was similar to the seed proteins such as 7S and 11S (Malhotra & Coupland, 2004), suggesting that these proteins were present on the surface of OBC, whereas the zeta-potential value of OB agreed with one in previous research (Iwanaga et al., 2007), indicating that the storage proteins are actually removed during alkaline extraction. The much higher zeta-potential value of OBC than OB cannot necessarily explain the tendency

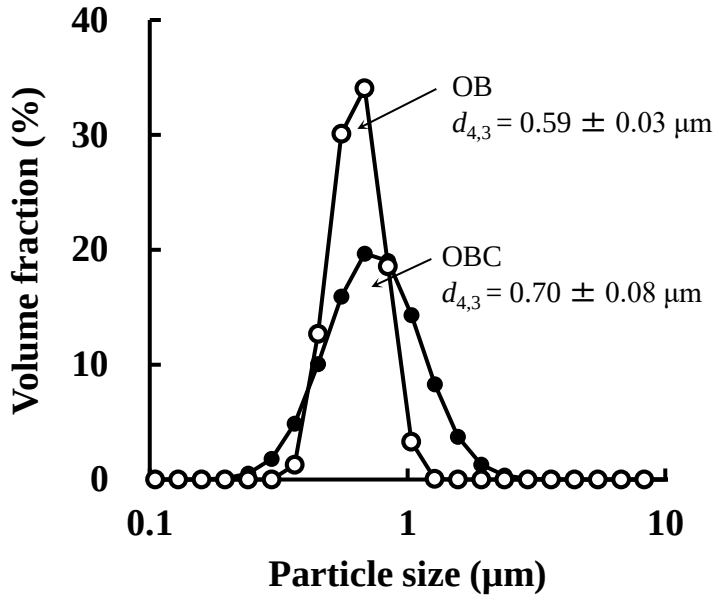

Fig. 1-1 Particle size distribution of OB (○) and OBC (●). Each sample was diluted by 10 mM sodium phosphate buffer solution (pH 7.0) and analyzed at a refractive index of 1.45.

of OBC to form aggregates and thereby suggests the presence of other attractive forces leading to the aggregation. A possible attractive force between the OBC is a hydrophobic interaction between storage seed proteins on the OBC surfaces such as 7S and 11S, which have strong tendency to aggregate without heat treatment as reported by Nik, Tosh, Poysa, Woodrow, & Corredig (2008). They reported that unheated soymilk included large aggregated structures containing protein and oil droplets using TEM.

To observe the microstructure of OB and OBC in detail, the sample dispersions containing 0.1 wt% of OB and OBC were subjected to STEM with negative staining to prevent destruction of the structure (Fig. 1-2). The images show that the individual particle size of OB and OBC generally corresponds to the particle size obtained from the distribution data in the previous section (Fig. 1-1). OBC was surrounded by a large number of gathered nano-ordered small particles (marked with *) (Fig. 1-2 (b)), while OB seemed to barely contain such small

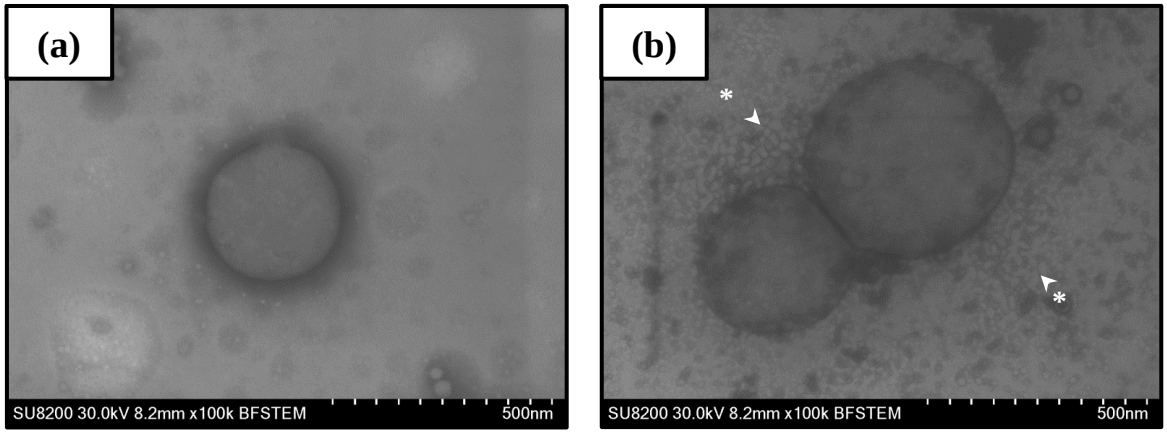

Fig. 1-2 STEM observation of OB (a) and OBC (b). Each sample was negatively stained using phosphotungstic acid (pH 7.0).

particles (Fig. 1-2 (a)). The results clearly show that the protein particles were present on the surface of OBC even after repeated centrifugation processes, probably leading to the susceptibility to aggregation between OBC discussed in the particle size analysis above. The particles were considered to be the nano-ordered protein particles (< 40 nm) consisting of seed storage proteins and other minor components abundantly present in unheated soymilk described by Ono, Choi, Ikeida, & Odagiri (1991). It is possible that such particles tend to extensively bridge oil droplets in OBC to form the aggregates over 1 μm observed in Fig. 1-1.

3.1.2 Protein profiles

Protein amounts and compositions of extracted oil bodies usually depend on their extraction pH conditions (Chen & Ono, 2010; Cao et al., 2015). To clarify the purity and the bridging proteins of OB and OBC, the author carried out the quantification and qualification of OB and OBC

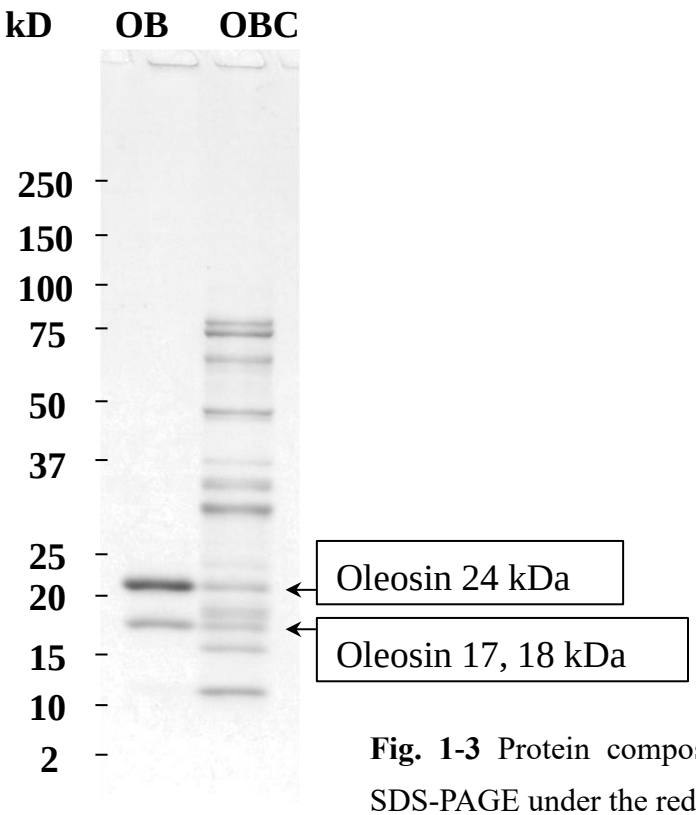

Fig. 1-3 Protein composition of OB and OBC analyzed by SDS-PAGE under the reduced condition.

proteins by BCA method and SDS-PAGE, respectively. The protein content of OB and OBC was 5.12 ± 0.22 wt% and 8.11 ± 0.62 wt% (dry weight basis), respectively, indicating that OBC contained larger amount of proteins than OB. Based on these values, approximately 3.0 wt% of extra proteins was adsorbed to oil droplets in OBC and can be eliminated by adjusting pH conditions. Calculating a protein surface load of OB and OBC according to the method described by McClements (1999), it was 4.1 ± 0.2 mg/m^2 and 6.7 ± 0.6 mg/m^2, respectively, indicating that the surface coverage of OBC was about 1.6 times thicker than that of OB. These thickness values are reasonable based on the literature by Dalgleish (2004). This difference could lead to different interfacial and emulsifying properties of OB and OBC to be examined in the following sections.

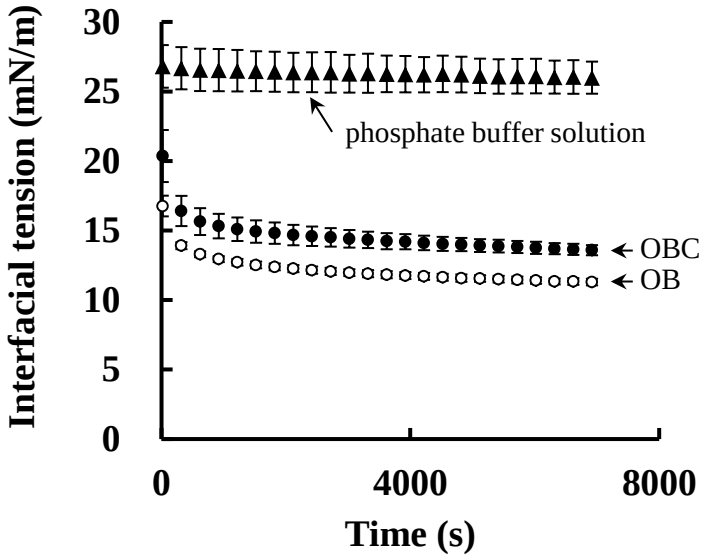

Fig. 1-4 The time-dependent interfacial tension between purified soybean oil and 1 wt% of OB and OBC dispersion. The interfacial tension between the purified oil and 10 mM phosphate buffer solution without the samples was measured as a blank. An aqueous drop was formed into the bulk oil phase and the interfacial tension was calculated from the drop shape. All measurements were conducted at 25°C (n = 3, mean ± S.D.).

Fig. 1-3 illustrates the protein composition of OB and OBC collected under the different pH conditions analyzed by SDS-PAGE. The protein composition of OB and OBC was obviously different from each other and mostly agrees with that in the previous researches (Cao et al., 2015; Chen & Ono, 2010). The author can confirm that well-purified OB without involved seed storage proteins and other minor components were collected. On the other hand, in addition to oleosins, OBC contained other proteins like 7S, 11S, allergen proteins, and trypsin inhibitor, indicating that these proteins were the nano-ordered protein particles observed as a surrounding part of OBC oil droplets (Fig. 1-2 (b)).

3.1.3. Interfacial properties of OB and OBC

Emulsifying ability of surface-active materials generally depends on adsorption kinetics at the O/W interface, in relation to diffusion rate and configuration of adsorbed compounds. To evaluate the adsorption kinetics of OB and OBC, interfacial tension at the dynamic interface between oil and aqueous phase was measured by the pendant drop method. Fig. 1-4 shows the time-dependent interfacial tension after droplet formation between bulk soybean oil purified with Florisil and the sample dispersions containing 1.0 wt% of OB and OBC in 10 mM phosphate buffer solutions (pH 7.0) at 25°C. The interfacial tension of the phosphate buffer solution used for sample dispersions was an almost constant value of 27 mN/m, ensuring the absence of surface-active impurities in both the oil and buffer solution phase. For the OB dispersion, at the initial measurement stage, the interfacial tension between oil and aqueous phases was significantly lower than that for the blank solution without OB, indicating that OB rapidly adsorbed onto the interface immediately after the droplet formation. These data correspond to the previous data obtained by Waschatko et al. (2012 (b)).

The interfacial tension of the OBC dispersion initially decreased in the time-dependent manner, which is almost the same as that of the OB dispersion, suggesting that OB and OBC diffused from the aqueous phase to the O/W interface at a similar rate. These results suggest that exogenous proteins such as 7S and 11S globulins do not disturb the adsorption of oil bodies to O/W interfaces and therefore tend to remain the oil body surfaces. As reported by Wilde (2000), the initial reduction of interfacial tension relates to the emulsifying ability of surface-active molecules like whey and egg proteins, therefore the materials studied in this work are expected to be utilized as an effective emulsifying agent. The interfacial tension for both OB and OBC time-dependently decreased and reached a plateau approximately after 1500 s, suggesting that the adsorption of OB and OBC onto O/W interface achieve the equilibrium state. At this stage, the interfacial tension for OB was obviously lower than that for OBC,

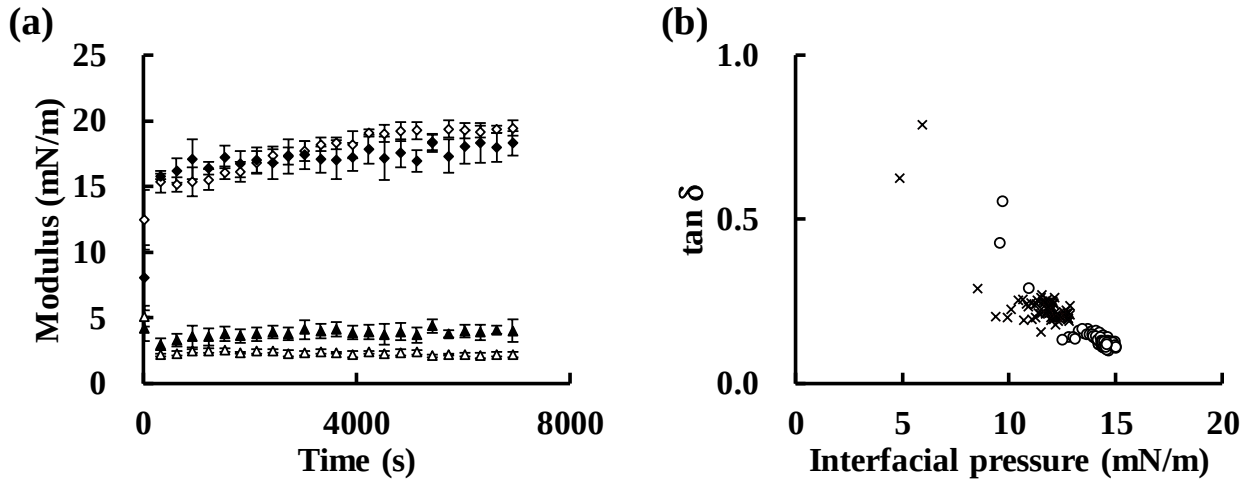

Fig. 1-5 (a) Interfacial viscoelasticity of OBC (filled symbols) or OB (open symbols). Rhomb symbols illustrates the storage modulus (E') and triangle symbols indicates the loss modulus (E"), respectively (n = 3, mean ± S.D.). (b) Loss tangent for OB (○) and OBC (×) was plotted as a function of the interfacial pressure (n = 3).

probably due to closer packing and/or deeper embedding of non-aggregated fine OB at the O/W interface compared to OBC aggregated with other proteins depending on the structural features such as size, shape etc. as discussed in Figs. 1-1 and 1-2 and/or depending on the different electrostatic repulsive forces as described in the result from zeta-potential measurements, that is, larger electrostatic repulsive force of adsorbed OBC may prevent the further adsorption of other OBC thereafter arriving at the interface. These facts maybe lead to different resistance of OB- and OBC-stabilized emulsions against oil droplet coalescence.

Another aspect affecting the resistance against oil droplet coalescence is the mechanical property of interfacial layer often represented by the viscoelasticity of the oil droplet surfaces consisting of adsorbed surface-active molecules. To analyze the viscoelasticity of the interface between oil and water composed of OB and OBC, the dynamic interfacial rheological measurements were performed by oscillating the interfacial area of the droplet containing OB and OBC. Fig. 1-5 (a) shows the storage modulus (E') and loss modulus (E") of

the interfacial layer formed with OB and OBC between the purified oil and the sample dispersion as a function of time. During initial stage of the measurements, E' of both the OB and OBC adsorbed interface steeply increased, while E" remained within a low level. E' of both the OB and OBC interface was thoroughly higher than E" throughout the measurements, indicating that OB and OBC formed elastic film at the O/W interface rather than viscous one. The numerical value of E' and E" of the OB interface was generally higher and lower than that of OBC, respectively.

Interfacial pressure-normalized loss tangent (tanδ) was calculated based on these results to estimate the viscoelasticity of the interface formed with OB and OBC independent from the amount of adsorption. Fig. 1-5 (b) shows the tanδ versus interfacial pressure curve obtained from the measurement of time-dependent changes of E' and E" of the interface shown in Fig. 1-5 (a). At the interfacial pressure of about 10.86 mN/m that is suitable for direct comparison of the viscoelasticity of the OB and OBC based interfaces under the same amount of adsorption and the analytically stable condition after where several minutes had passed since droplet creation, tanδ of the OB and OBC interfaces was of similar values 0.290 and 0.243, respectively. The viscoelasticity of the OB interface was 1.19 times as high as that of the OBC one, indicating that viscoelasticity of the OB and OBC interfaces was not so different when they were present at the O/W interface with the same concentration. Considering the equilibrium state of the O/W interface composed of OB and OBC, however, the density of adsorbed OB at the interface was much larger than that of OBC (Fig. 1-4). For relating the results of Fig 1-5 (b) to the stability of actual emulsions, the comparison of tanδ should be carried out for the protective layer ultimately or maximum adsorbed. Therefore, tanδ value at the maximal interfacial pressure was tried to be compared. However, because of the fluctuation

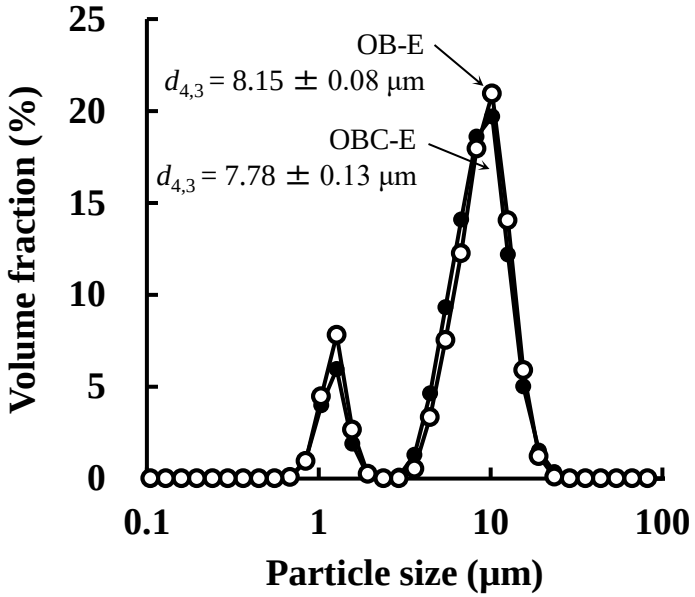

Fig. 1-6 Particle size distribution of OB- and OBC-stabilized emulsion (OB-E (○) and OBC-E (●)). The $d_{4,3}$ was calculated from the larger peak (>1.57 mm) of each particle size distribution.

of tanδ value, the value at the maximal interfacial pressure did not necessarily represent the minimum value of tanδ. Alternatively the minimum value of tanδ was employed for the comparison in this case, since the minimum value reflects the potential viscoelasticity of adsorbed layer. The minimum tanδ value of the OB and OBC interfaces was 0.102 and 0.191, respectively. The viscoelasticity of the OB interface was 0.53 times as high as that of the OBC interface. It means that the interface consisting of OB behaved as much more solid-like materials than OBC, suggesting that OB-stabilized emulsions are more stable against droplet coalescence than OBC-stabilized ones.

3.2. Application of OB and OBC as an emulsifying agent

3.2.1. Characteristics of OB-E and OBC-E

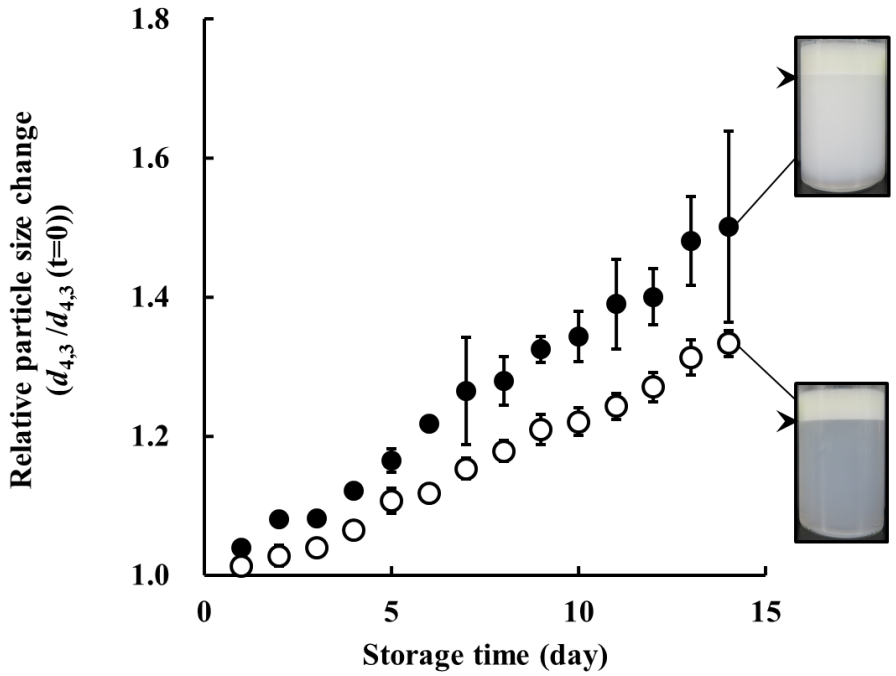

Fig. 1-7 Relative particle size change of OB-E (○) and OBC-E (●). Each sample was stored at room temperature with 0.02% (w/v) of sodium azide.

To examine emulsifying ability of OB and OBC as an emulsifying agent, I prepared emulsions (OB-E and OBC-E) by mixing the sample dispersions and the soybean oil treated with Florisil to measure their droplet size distribution. Fig. 1-6 illustrates the particle size distribution of OB-E and OBC-E just after the emulsification process. The particle size distribution of both OB-E and OBC-E had the two small and large major peaks at the sizes of 0.5 - 1.5 μm and 1.5 - 20.0 μm. The former peak was attributed to OB and OBC, whilst the latter peak was assigned to emulsion oil droplets stabilized by OB and OBC. The former OB and OBC peak slightly shifted from the original position via the agitation necessary for emulsification due to coalescence. This phenomenon was confirmed using the OB and OBC dispersions without any added oils (data not shown). The particle size distribution of OB-E and OBC-E were almost the same, although the statistical difference was detected for the mean diameter calculated from the larger peaks, $d_{4,3}$ (*t*-test, $p < 0.05$), maybe based on the similar diffusion rate of OB and OBC to the O/W

interface. As shown in Fig. 1-4, the initial rapid decline of interfacial tension according to time occurred similarly to OB and OBC, suggesting that OB and OBC diffused from the aqueous phase to the O/W interface at a similar rate.

To evaluate the stability of OB-E and OBC-E against coalescence, visual observation and particle size measurements were conducted for 2 weeks at room temperature. The visual observation indicated that oil droplets in both OB-E and OBC-E creamed and separated into two cream-rich and opaque serum layers after 24 h (data not shown), while destabilized free oil was not observed for both emulsions after 2 weeks storage (Fig. 1-7). This means that OB-E and OBC-E are unstable against creaming and stable against macroscopic severe coalescence leading to free oil separation. The relative change of mean particle size was calculated for OB-E and OBC-E to directly compare the stability of these emulsions against coalescence in a micro-ordered scale. The mean particle size of both OB-E and OBC-E slightly increased, while the increasing rate of OBC-E was larger than that of OB-E, that shows OB-E was more stable than OBC-E against oil droplet coalescence. The author confirmed that the increase was based on coalescence not on aggregation by ultrasonication and additional SDS (data not shown). To consider mechanisms for the different stability, zeta-potential of OB-E and OBC-E oil droplets was additionally measured as was done for OB and OBC in section 3.1.1. Resultantly, the zeta-potential of OB-E and OBC-E was -21.9 ± 1.8 mV and -31.6 ± 0.5 mV, respectively, similar to the results from OB and OBC alone. The results suggest that the major factor determining the stability of OB- and OBC-based emulsions against coalescence is the mechanical strength of the interfacial adsorbed layer discussed in section 3.1.3 rather than the electrostatic repulsion force between the emulsion oil droplets. The reason why the mechanical strength was more dominant for the emulsion stability than the electrostatic repulsive force is possibly that condensed oil droplets of OB-E and OBC-E in the creamed layer contacted each

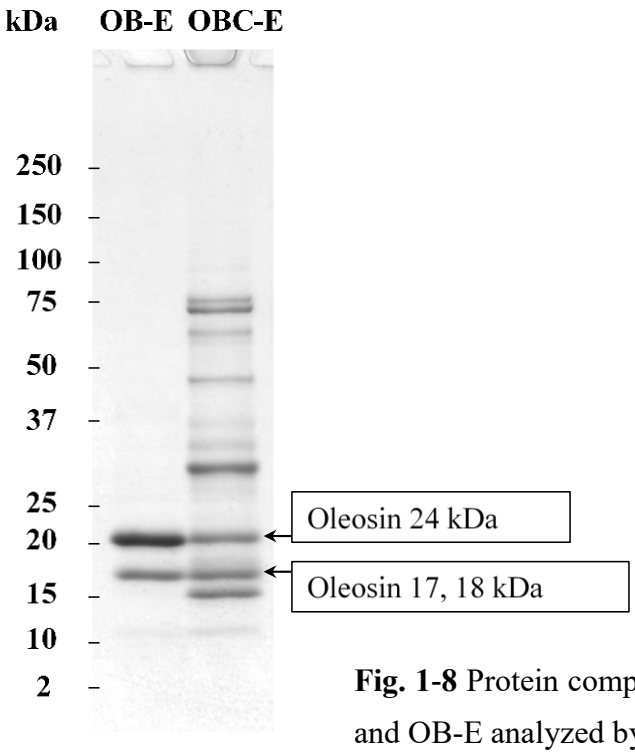

Fig. 1-8 Protein composition of adsorbed proteins in both OBC-E and OB-E analyzed by SDS-PAGE under the reduced condition.

other so that the electrostatic repulsive force effective for keeping the distance between droplets no longer contributed to stabilizing the emulsions.

3.2.2. Analysis of oil droplet surface

The above discussion made for the zeta-potential of OB-E and OBC-E implies that the surface protein composition of the emulsions reflects that of original OB and OBC, and in the latter, other proteins such as 7S and 11S inevitably adsorbed onto the droplet surface. The surface proteins adsorbed onto the emulsion droplets were collected via the gentle centrifugation and then subjected to the BCA method and SDS-PAGE. The surface protein load of OB-E and OBC-E was 2.4 ± 0.0 mg/m^2 and 3.6 ± 0.2 mg/m^2, respectively, which was of almost the same ratio compared to that of OB and OBC. This fact suggests that the surface composition of OB-E and OBC-E corresponds to that of original OB and OBC. Fig. 1-8 illustrates the protein composition of the adsorbed materials on OB-E and OBC-E oil droplets analyzed by

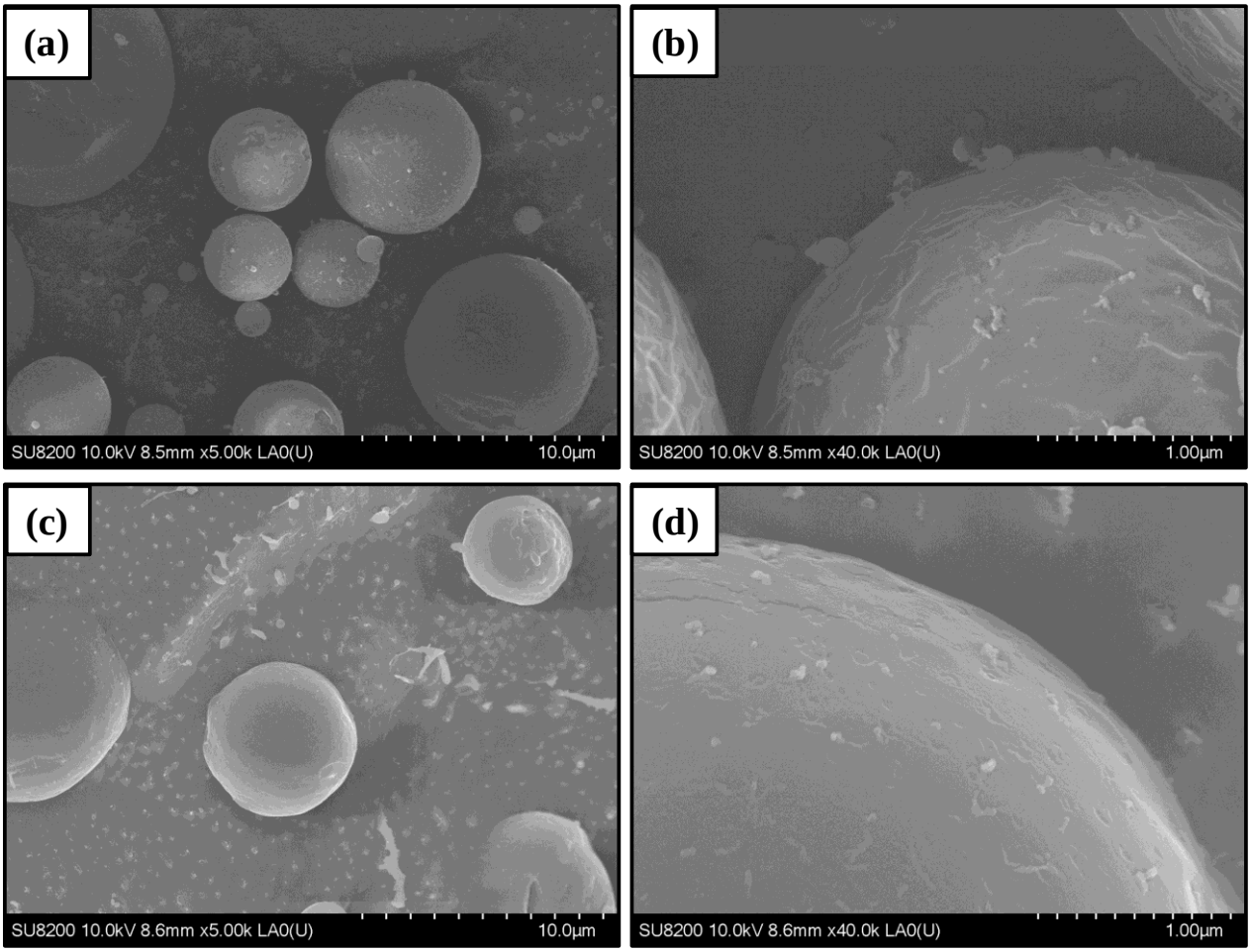

Fig. 1-9 Cryo-SEM observation of OB-E (a and b) and OBC-E (c and d). The left images were taken at low magnification (5000 times) and the right images were at high magnification (40,000 times).

SDS-PAGE. Analyses of the adsorbed protein revealed that the storage proteins exactly adsorbed onto the oil droplet surface of OBC-E, while most of the adsorbed proteins on the OB-E droplet surface were oleosins (Fig. 1-8). Comparing Fig. 1-3 and Fig. 1-8, the protein profiles were similar to each other for OB and OBC. The results clearly showed that the whole proteins on the surface of OB and OBC non-specifically adsorbed to the newly-created oil droplet surfaces of OB-E and OBC-E without eliminated non-adsorbed proteins. Oil droplets of OBC-E therefore have a strong tendency to flocculate throughout the bridging action of storage

and other minor proteins as discussed in section 3.1.1, leading to increased droplet coalescence of OBC-E compared to OB-E described in section 3.2.1.

Through the above sections, the author revealed that OB and OBC non-specifically adsorbed to the OB-E and OBC-E oil droplet surfaces and probably formed single layer at the O/W interface in an intact or collapsed state. Waschatko et al. (2012 (a)) and Waschatko et al. (2012 (b)) previously reported that OB presumably adsorb to the A/W interface in the intact state first and subsequently collapse to cover the interface. To clarify whether OB and OBC adsorb onto the O/W interface of the emulsions in the intact or collapsed state, Cryo-SEM was conducted to observe the surface structure of OB-E and OBC-E droplets. Fig. 1-9 (a) and (c) depicts the microstructure of OB-E and OBC-E observed by Cryo-SEM at a low magnification. There were oil droplets etched from frozen continuous aqueous phase by sublimation. The particle size of both OB-E and OBC-E corresponds to the results from the particle size analysis of OB-E and OBC-E. Fig. 1-9 (b) and (d) show the magnified image of the OB-E and OBC-E droplet surfaces. Both the emulsion droplet surfaces were free from particles like the original oil bodies. These results suggest that most of the OB and OBC particles adsorbed to the O/W interface and then rapidly ruptured due to high shear rate homogenization. In such situation, the surface proteins and phospholipids of OB and OBC spread to the new O/W interface and the core lipids merged into the added dispersed soybean oil phase during emulsification process under the high-shear stresses.

4. References

Amine, C., Dreher, J., Helgason, T., & Tadros, T. (2014). Investigation of emulsifying properties and emulsion stability of plant and milk proteins using interfacial tension and interfacial elasticity. Food Hydrocolloids, 39, 180–186.

Cao, Y., Zhao, L., Ying, Y., Kong, X., Hua, Y., & Chen, Y. (2015). The characterization of soybean oil body integral oleosin isoforms and the effects of alkaline pH on them. Food Chemistry, 177, 288–294.

Chen, B., McClements, D. J., Gray, D. A., & Decker, E. A. (2012). Physical and oxidative stability of pre-emulsified oil bodies extracted from soybeans. Food Chemistry, 132(3), 1514–1520.

Chen, Y., Cao, Y., Zhao, L., Kong, X., & Hua, Y. (2014). Macronutrients and Micronutrients of Soybean Oil Bodies Extracted at Different pH. Journal of Food Science, 79 (7), 1285–1291.

Chen, Y. & Ono, T. (2010). Simple Extraction Method of Non-allergenic Intact Soybean Oil Bodies That Are Thermally Stable in an Aqueous Medium. Journal of Agricultural and Food Chemistry, 58 (12), 7402–7407.

Chove, B. E., Grandison, A. S., & Lewis, M. J. (2001). Emulsifying properties of soy protein isolate fractions obtained by isoelectric precipitation. Journal of the Science of Food and Agriculture, 81 (8), 759–763.

Deleu, M., Vaca-Medina, G., Fabre, J. F., Roiz, J., Valentin, R., & Mouloungui, Z. (2010). Interfacial properties of oleosins and phospholipids from rapeseed for the stability of oil bodies in aqueous medium. Colloids and Surfaces B: Biointerfaces, 80 (2), 125–132.

Dalgleish, D. G. (2004). Food emulsions: Their structures and properties, Food emulsion fourth edition revised and expanded, p.1–44, Marcel Dekker, Inc.

Fisk, I. D. & Gray, D. A. (2011). Soybean (Glycine max) Oil Bodies and Their Associated Phytochemicals. Journal of Food Science, 76 (9), 1349–1354.

Huang, A. H. C. (1992). Oil Bodies and Oleosins in Seeds. Annual Review of Plant Physiology and Plant Molecular Biology, 43 (1), 177–200.

Hu, M., McClements, D. J., & Decker, E. A. (2003) Lipid Oxidation in Corn Oil-in-Water Emulsions Stabilized by Casein, Whey Protein Isolate, and Soy Protein Isolate. Journal of Agricultural and Food Chemistry, 51, 1696–1700.

Iwanaga, D., Gray, D. A., Fisk, I. D., Decker, E. A., Weiss, J., & McClements, D. J. (2007). Extraction and characterization of oil bodies from soy beans: A natural source of pre-emulsified soybean oil. Journal of Agricultural and Food Chemistry, 55 (21), 8711–8716.

Jolivet, P., Boulard, C., Beaumal, V., Chardot, T., & Anton, M. (2006). Protein components of low-density lipoproteins purified from hen egg yolk. Journal of Agricultural and Food Chemistry, 54 (12), 4424–4429.

Karaka, A. C., Low, N. H., & Nickerson, M. T. (2015). Potential use of plant proteins in the microencapsulation of lipophilic materials in foods. Trends in Food Science & Technology, 42, 5–12.

Kapchie, V. N., Towa, L. T., Hauck, C., & Murphy, P. A. (2010). Evaluation of enzyme efficiency for soy oleosome isolation and ultrastructural aspects. Food Research International, 43 (1), 241–247.

Keerati-u-rai, M. & Corredig, M. (2009). Heat-induced changes in oil-in-water emulsions stabilized with soy protein isolate. Food Hydrocolloids, 23 (8), 2141–2148.

Keerati-U-Rai, M. & Corredig, M. (2010). Heat-induced changes occurring in oil/water emulsions stabilized by soy glycinin and β-conglycinin. Journal of Agricultural and Food Chemistry, 58 (16), 9171–9180.

Kiosseoglou, V. & Sherman, P. (1983). Influence of egg yolk lipoproteins on the rheology and stability of oil/water emulsions and mayonnaise 1. Viscoelasticity of groundnut oil-in-water emulsions and mayonnaise. Journal of Texture Studies, 14 (4), 397–417.

Laemmli, U. K. (1970). Nature, 227, 680–685.

Liu, K. (1997). Agronomic characteristics, production, and marketing, Soybeans: chemistry, technology and utilization, p. 1–24, Chapman & Hall.

Malhotra, A. & Coupland, J. N. (2004). The effect of surfactants on the solubility, zeta potential, and viscosity of soy protein isolates. Food Hydrocolloids, 18 (1), 101–108.

Martinet, V., Saulnier, P., Beaumal, V., Courthaudon, J. L., & Anton, M. (2003). Surface properties of hen egg yolk low-density lipoproteins spread at the air–water interface. Colloids and Surfaces B: Biointerfaces, 31 (1-4), 185–194.

Maurer, S., Waschatko, G., Schach, D., Zielbauer, B. I., Dahl, J., Weidner, T., Bonn, M., Vilgis, T. A. (2013). The role of intact oleosin for stabilization and function of oleosomes. The Journal of Physical Chemistry. B, 117 (44), 13872–83.

McClements, D. J. & Gumus. C. E. (2016). Natural emulsifiers — Biosurfactants, phospholipids, biopolymers, and colloidal particles: Molecular and physicochemical basis of functional performance. Advances in Colloid and Interface Science, 234, 3–26.

McClements, D. J. (1999). Characterization of emulsion properties, Food Emulsions: Principles, Practice, and Techniques first edition, p. 297–337, CRC Press LCC.

Mine, Y. (1998). Adsorption Behavior of Egg Yolk Low-Density Lipoproteins in Oil-in-Water Emulsions. Journal of Agricultural and Food Chemistry, 46 (1), 36–41.

Molina, E., Papadopoulou, A., & Ledward, D. A. (2001). Emulsifying properties of high pressure treated soy protein isolate and 7S and 11S globulins. Food Hydrocolloids, 15 (3), 263–269.

Murphy, R. W., Farkas, B. E., & Jones, O. G. (2016). Dynamic and viscoelastic interfacial behavior of β-lactoglobulin microgels of varying sizes at fluid interfaces. Journal of Colloid and Interface Science, 466, 12–19.

Nik, M. A., Tosh, S., Poysa, V., Woodrow, L., & Corredig, M. (2008). Physicochemical characterization of soymilk after step-wise centrifugation. Food Research International, 41 (3), 286–294.

Nikiforidis, C. V., Ampatzidis, C., Lalou, S., Scholten, E., Karapantsios, T. D., & Kiosseoglou, V. (2013). Purified oleosins at air–water interfaces. Soft Matter, 9 (4), 1354–1363.

Nikiforidis, C. V. & Kiosseoglou, V. (2009). Aqueous Extraction of Oil Bodies from Maize Germ (Zea mays) and Characterization of the Resulting Natural Oil-in-Water Emulsion. Journal of Agricultural and Food Chemistry, 57, 5591–5596.

Ono, T., Choi, M. R., Ikida, A., & Odaoiri, S. (1991). Changes in the Composition and Size Distribution of Soymilk Protein Particles by Heating. Agricultural and Biological Chemistry, 55 (9), 2291–2297.

Palazolo, G. G., Mitidieri, F. E., & Wagner, J. R. (2003). Relationship between Interfacial Behaviour of Native and Denatured Soybean Isolates and Microstructure and Coalescence of Oil in Water Emulsions - Effect of Salt and Protein Concentration. Food Science and Technology International, 9 (6), 409–419.

Palazolo, G. G., Sobral, P. A., & Wagner, J. R. (2011). Freeze-thaw stability of oil-in-water emulsions prepared with native and thermally-denatured soybean isolates. Food Hydrocolloids, 25 (3), 398–409.

Palazolo, G. G., Sorgentini, D. A., & Wagner, J. R. (2005). Coalescence and flocculation in o/w emulsions of native and denatured whey soy proteins in comparison with soy protein isolates. Food Hydrocolloids, 19 (3), 595–604.

Pimentel, D. & Pimentel, M. (2003). Sustainability of meat-based and plant-based diets and the environment, The American Journal of Clinical Nutrition, 78 (suppl), 660S–3S

Pimentel, D., Williamson, S., Alexander, C. E., Pagan, O. G., Kontak, C., & Mulkey, S. E. (2008). Reducing energy inputs in the US food system. Human Ecology, 36, 459–471.

Rayner, M. (2015). Current status on novel ways for stabilizing food dispersions by oleosins, particles and microgels. Current Opinion in Food Science, 3, 94–109.

Rodrigues, I. M., Coelho, J. F. J., & Carvalho, M. G. V. S. (2012). Isolation and valorization of vegetable proteins from oil seed plants: Methods, limitations and potential. Journal of Food Engineering, 109, 337-346.

Samoto, M., Maebuchi, M., Miyazaki, C., Kugitani, H., Kohno, M., Hirotsuka, M., & Kito, M. (2007). Abundant proteins associated with lecithin in soy protein isolate. Food Chemistry, 102 (1), 317–322.

Tzen, J. T., & Huang, A. H. C. (1992). Surface structure and properties of plant seed oil bodies. The Journal of Cell Biology, 117 (2), 327–335.

Waschatko, G., Junghans, A., & Vilgis, T. A. (2012 (a)). Soy milk oleosome behaviour at the air – water interface. Faraday Discussions, 158, 1–13.

Waschatko, G., Schiedt, B., Vilgis, T. A., & Junghans, A. (2012 (b)). Soybean Oleosomes Behavior at the Air − Water Interface. Journal of Physical Chemistry B, 116, 10832–10841.

Wijesundera, C., Boiteau, T., Xu, X., Shen, Z., Watkins, P., & Logan, A. (2013). Stabilization of fish oil-in-water emulsions with oleosin extracted from canola meal. Journal of Food Science, 78 (9), 1340–1347.

Wilde, P. J. (2000). Interfaces: Their role in foam and emulsion behaviour. Current Opinion in Colloid and Interface Science, 5 (3-4), 176–181.

White, D.A., Fisk, I.D., Mitchell, J.R. Wolf, B., Hill, S.E., & Gray, D.A. (2008). Sunflower-seed oil body emulsions: Rheology and stability assessment of a natural emulsion. Food Hydrocolloids, 22, 1224–1232.

Wu, N. N., Huang, X., Yang, X. Q., Guo, J., Zheng, E. L., Yin, S. W., Zhu, H. J., Qi, J. R. He, X. T., & Zhang, J. B. (2012). Stabilization of soybean oil body emulsions using ι-carrageenan: Effects of salt, thermal treatment and freeze-thaw cycling. Food Hydrocolloids, 28 (1), 110–120.

Wu, N. N., Yang, X. Q., Teng, Z., Yin, S. W., Zhu, J. H., & Qi, J. R. (2011). Stabilization of soybean oil body emulsions using κ, ι, λ-carrageenan at different pH values. Food Research International, 44 (4), 1059–1068.

Chapter 2:
Effects of acid and salt addition on the colloidal and emulsifying properties of soybean oil bodies

1. Introduction

Many food products such as dressings and sauces exist as an oil-in-water (O/W) emulsion, where oil droplets disperse in an immiscible aqueous continuous phase (McClements, 2016). These emulsified food products are usually manufactured by homogenizing oil and water phases mainly with natural animal-derived proteins derived from milk and egg yolk as indispensable amphiphilic emulsifiers occasionally together with small molecule surfactants enhancing long-term stability and imparting bacteriostatic effects (McClements, 2016; Kato & Shibasaki, 1975). On the other hand, consumers' demands for their daily food products are increasingly diversifying nowadays based on the development of cultural diversity and the increased interest in health matters: natural, non-allergic, health-beneficial, vegetarian-friendly, religiously-acceptable, etc. In addition to this, production of animal proteins generally expends much more energy and resources compared to that of plant ones (Pimentel & Pimentel, 2003). It is of critical importance to establish novel plant-based emulsifiers that can be practically utilized as counterparts of the conventional animal proteins to build a sustainable society.

In this context, the author previously studied soybean oil bodies (OBs), a submicron oil-storing complex organelle in the seed, which consists of neutral lipids at the core and surrounding polar lipids and membrane proteins named oleosins (Huang, 1992), to develop an effective plant-based emulsifier as a substitute of the conventional animal-based ones, owing to a fact that the structural and compositional features of OB are apparently similar to egg yolk lipoproteins predominantly responsible for its high-functional emulsifying ability (Hatta, Hagi,

& Hirano, 1997). The author compared emulsifying properties of crude OBs extracted under neutral conditions inevitably coupled with other storage globular proteins, e.g., glycinin and β-conglycinin through attractive interactions and purified OBs further isolated from the involved globular proteins under alkaline conditions at pH 11, and resultantly revealed that both of the crude and purified OBs dispersed in a neutral pH continuous aqueous media containing no added salts possessed similar emulsifying ability, while the purified OBs formed more physically stable emulsions particularly for oil droplet coalescence (Ishii et al., 2017). In order to achieve industrial application of purified OBs to food emulsions like dressings often stabilized by egg yolk (Hatta et al., 1997), effects of acids and salts addition, typically acetic acid and NaCl formulation for the condiments and their combinational effects on the emulsifying properties of purified OBs should be clarified, since oleosin proteins comprising amino acid residues with various side chains present on the surface of OBs with an isoelectric point of 5.5 – 6.0 (Chen & Ono, 2010) tend to change in their electrically charged states due to the screening actions of acids and salts in the acidic environment and thereby change in conformation and solubility in the aqueous phase, possibly leading to flocculation or aggregation of OBs via the attractive hydrophobic interactions.

The emulsifying ability of emulsifiers can be considered based on competing two phenomena, i.e., creation and re-coalescence of oil droplets during emulsification of oil and water. Creation efficiency of oil droplets generally depends on the adsorption rate of an emulsifier to newly-formed oil surfaces via diffusion through the electrostatic energetic barrier, whereas re-coalescence resistance is presumably determined by both packing of adsorbed emulsifiers at the interfaces and electrostatic repulsion between approaching oil droplets. Since these two phenomena concurrently occurring during emulsification seem to be highly affected by the particle size and electrical charge of OBs sensitively influenced by pH and salt

concentration conditions as mentioned above, acids and salt addition should result in significantly different emulsifying properties of OBs.

Since the interface between immiscible oil and water is thermodynamically unstable, the emulsified oil droplets covered by adsorbed emulsifiers are still thermodynamically metastable (Walstra, 2003; McClements, 2016). The kinetically-stabilized droplets therefore inevitably undergo undesirable physical phenomena such as creaming, flocculation, and coalescence (McClements, 2016). Among these physical phenomena, coalescence is irreversible eventually leading to free oil release, and therefore particularly unfavorable for dressing-like products often shaken before serving. The resistance of protein-based O/W emulsions against oil droplet coalescence is predominantly determined based on collision frequency of oil droplets and mechanical strength of the adsorbed protective layer on the oil droplet surfaces estimated by inter-droplet repulsive potential and interfacial viscoelasticity, respectively. The acid and salt addition may influence both colloidal interaction between OB-adsorbed oil droplets and molecular interaction of OB-consisting molecules at the interfacial adsorbed films on the emulsion oil droplet surfaces.

The objective of this chapter is to clarify the effects of acid and salt addition on colloidal and emulsifying properties of OBs towards practical application. The dispersed states of OBs in acetic acid buffer solutions (pH 4.0 – 5.5) or phosphate buffer solutions (pH 7.0, control) containing 0, 50, and 100 mM NaCl, respectively, were analyzed by particle size and zeta potential measurements. The adsorption kinetics to an oil-water interface and rheological properties of adsorbed films at the interface was analyzed based on tensiometry. Emulsifying activity of OBs and physical stability of resultant OB-stabilized O/W emulsions were evaluated by particle size analysis immediately after preparation and periodical measurements during storage, respectively.

2. Materials and Methods

2.1 Materials

Commercial soybean seeds (Glycine max (L.) Merr, “Tamahomare”) were purchased from a local market. Ultrapure water was used for preparation of all samples, buffer solutions, and reagents. Florisil was bought from Sigma. Other chemical agents were of experimental grade.

2.2 Preparation of soybean oil body (OB) dispersions

OBs were extracted from the soybean seeds via the simple aqueous extraction method under an alkaline condition according to Chen & Ono (2010) with slight modifications described in the previous work (Ishii et al., 2017). The soybean seeds (50 g) were soaked in excessive ultrapure water (approximately 300 ml) at 4°C for 18 hours. The soaked soybeans were homogenized with 200 ml of water by a mixer, and then the homogenate was filtrated through three layers of gauze to obtain raw soymilk (approximately 200 ml). The soymilk was mixed with sucrose to achieve the final concentration of 20 wt% and the pH value was simultaneously adjusted to 11.0 using 1.0 M of sodium hydroxide. After centrifugation by a centrifuge at 22,140×g for 30 min at 4°C, a floating cream layer was carefully collected from the sample. The collected cream layer was dispersed into sucrose-sodium hydroxide solution (20 wt% sucrose, pH 11.0) and recentrifuged under the same conditions to remove external components that did not interact with oil body surfaces; This washing process was repeated once again. The cream layer was further washed two times using 10 mM of sodium phosphate buffer solution (pH 7.0) to eliminate sucrose from the cream layer. The washed cream layer was finally dispersed into the phosphate buffer solution and stirred overnight on a magnetic stirrer to ensure well-dispersed states.

An aliquot of the OB dispersion (3 ml) was treated with a heat-drying process (130°C,

3 hours) for determination of a dry weight of the dispersion. Based on the dry weight concentration, the original OB dispersion was diluted using to 10 mM sodium acetate buffer solutions (pH4.0, pH4.5, pH5.0, and pH5.5) or 10 mM sodium phosphate buffer solutions (pH 7.0) containing 0 mM, 50 mM, and 100 mM of additional sodium chloride, respectively, to achieve appropriate final dry weight-based concentrations in the following experiments.

2.3 Particle size analysis of OB

Particle size of OBs under the various aqueous condition was determined by a laser-diffraction particle size analyzer (SALD 2200, Shimadzu Co., Japan). OBs were dispersed in to a sample dispersing chamber filled with the buffer solutions (pH 4.0, 4.5, 5.0, 5.5, and 7.0; NaCl concentration of 0, 50, and 100 mM, respectively) and measured at the refractive index of 1.45. To clarify presence of aggregated particles, 10 wt% SDS solution was subsequently poured into the diluted OB dispersions in the chamber, followed by remeasurement.

2.4 Zeta-potential measurements of OB

Zeta-potential of OBs in the various aqueous media was analyzed using a laser-Doppler zeta-potential analyzer (ELS-Z1, Otsuka Electronics Co. Ltd., Japan). The OB dispersions was appropriately diluted (about 2000 times) using the buffer solutions, respectively. Measurements were carried out at 25°C and automatically repeated 5 times for every sample.

2.6 Dynamic interfacial tension analysis at oil-water interface

2.6.1 Purification of soybean oil

Polar impurities such as free fatty acids and di- or mono-acyl glycerides were removed from soybean oil as described in the previous literature (Ishii et al., 2017). Florisil was dispersed to

soybean oil to achieve the final concentration of 4 wt% using a magnetic stirrer for 30 minutes, and the soybean oil was centrifuged at 22,140×g for 30 min to remove Florisil particles. The obtained purified soybean oil was stored in a shade bottle at room temperature before the following experiments.

2.6.2 Analysis of adsorption kinetics

Dynamic interfacial tension of between the purified oil and the 0.1 wt% OB dispersions was analyzed using a pendant drop tensiometer (Tracker, Teclis, France). Approximately 25 ml of the purified soybean oil was poured into a glass cell, and a needle tip of a micro syringe filled with the sample dispersions was immersed into the bulk oil phase. An aqueous droplet was created from the needle tip into the bulk oil phase, and based on the drop shape, interfacial tension was calculated. The droplet surface area was controlled at 30 mm^2 during the measurements (25°C, 7200 s). The adsorption rates and final adsorbed amounts were obtained by linear correlation at the steepest point of the trends and calculation of mean values of ten data points at the last.

2.7 Preparation of OB-stabilized emulsions

The dispersions including 1 wt% of OBs (24 g) and soybean oil (6 g) were coarsely homogenized by a high speed blender (Physcotron, Microtec, Japan) with NS-20 shaft at 15,000 rpm for 3 min, and subsequently processed with a ultrasonic homogenizer (Q700 Sonicator, Qsonica, L.L.C, USA) attached with a 1/2 inch probe at 30% intensity for 3 min to obtain OB-stabilized emulsions. During the ultrasonication, the sample tubes were immersed in an ice-water bath to prevent heat degradation. The size distribution of emulsified oil droplets in OB-stabilized emulsions were measured immediately after emulsification using the particle size

analyzer.

2.8 Evaluation of physical stability of OB-stabilized emulsions

The obtained emulsions containing sodium azide (0.02% (w/v)) as an antimicrobial agent were stored at 25°C and subjected to periodical particle size analysis with/without SDS by the same method described in the section 2.3 to evaluate oil droplet flocculation and coalescence. The relative particle size changes according to the following equation are presented:

$$\text{Relative particle size change} = \frac{d_{4,3}}{d_{4,3}\ (\text{day } 0)}$$

, where $d_{4,3}$ is the volume-based mean particle size.

2.9 Statistical analysis

All sample preparation and analysis were at least triplicated. The obtained values were presented as means ± standard deviations based on the triplicated experiments. Representative results were depicted for time-dependent interfacial tension analysis and emulsion particle size analysis. All statistical analyses were conducted using Microsoft Excel version 2016.

3. Results & Discussion

3. Results & Discussion

3.1 Colloidal properties of soybean OBs under the various aqueous conditions

To characterize pH-dependent aggregation behavior of OBs, particle size measurements were performed between pH 4.0 and 7.0 containing various amounts of NaCl (0 mM, 50 mM, and 100 mM, respectively). Fig. 2-1 shows volume-based mean particle size of OBs. At NaCl concentration of 0 mM (black symbols), the mean particle size increased at pH 5.0 and 5.5, suggesting that the net charge of OB particles probably approached to zero around pH 5.5. This results largely agrees with other studies that investigated dispersibility of OBs (Chen & Ono, 2010), whereas the pH value of 5.5 is slightly far from pI of major storage proteins in soybeans around pH 4 – 5 (Nishinari, Fang, guo, & Phillips, 2014), confirming that such globular proteins hardly consist of the OB surfaces and were almost negligible. At the NaCl concentration of 50 mM, the mean particle size increased around the same pH range, whereas at that of 100 mM, the pH-dependent changes were not significant.

To clarify whether the particle size increase is owing to aggregation/flocculation or coalescence of OBs, a SDS solution was applied into the sampling chamber after each measurement without SDS. All the large particles observed in the particle size analyses without SDS resultantly dissociated into submicron particles under all the conditions where the mean particle size increased (data not shown), indicating that the particle size increase was mostly due to aggregation/flocculation of dispersed OBs and suggesting the OB surface membranes consisting of oleosins and phospholipids are highly resistant against coalescence even though OB particles are contacting each other.

The pH-dependent aggregation observed around pH 5.0 and 5.5 probably results from reduction of electrostatic repulsive forces between OB particles. To estimate the electric charge

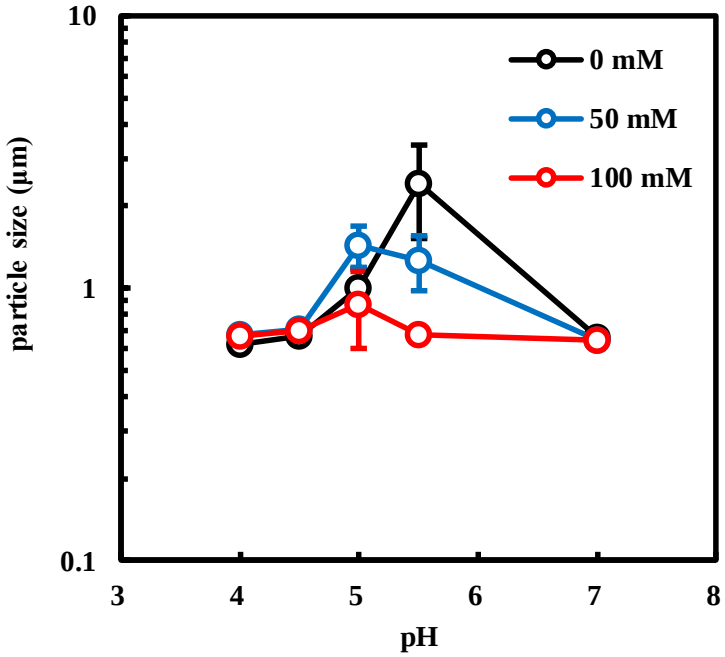

Fig. 2-1 pH-dependent change of volume-based mean particle size of OBs under different NaCl concentrations (0, 50, and 100 mM, respectively).

of the OB surfaces in the various aqueous media, zeta-potential of OBs was analyzed under the various conditions. Fig. 2-2 illustrates pH-dependent changes of zeta-potential values under the three NaCl concentrations (0 mM, 50 mM, and 100 mM). At the lowest NaCl concentration (black symbols), OB particles strongly charged negatively at pH 4.0 (approximately -40 mV), and the charge gradually reduced along with the pH increase, approached close to zero at pH 5.5 among all the analyzed pH values, and reached to a negative value at the neutral pH. The absolute zeta-potential values at pH 5.0 and 5.5 were less than 30 mV, a value critically required for prevention of aggregation/flocculation of colloidal particles (Dukhin & Goetz, 1998), indicating that the pH-dependent aggregation/flocculation of OBs at these pH values can be attributed to insufficient electrostatic repulsion.

Compared to the zeta-potential shift at NaCl concentration of 0 mM, the pH-dependent

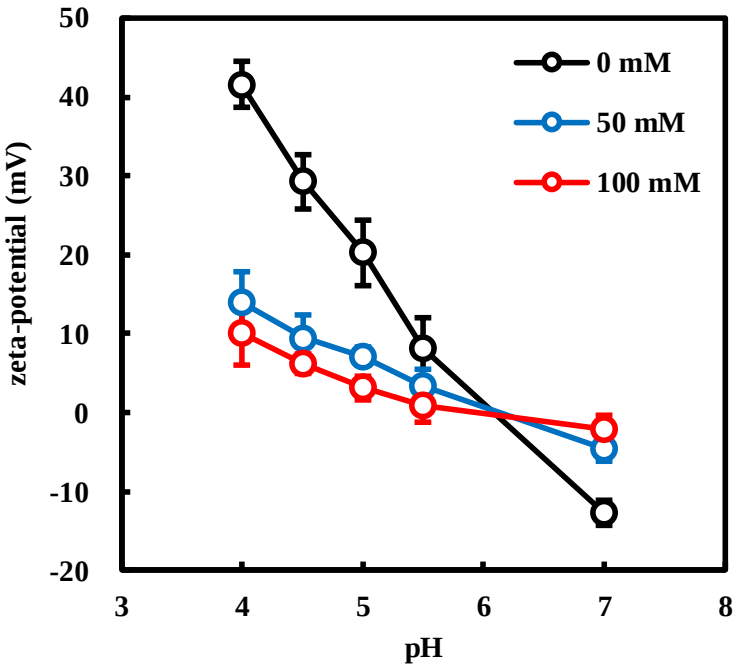

Fig. 2-2 pH-dependent change of Zeta-potential of OBs under different NaCl concentrations (0, 50, and 100 mM, respectively).

zeta-potential changes step-wisely declined by the increase of NaCl concentrations (blue and red symbols) presumably due to screening effects. Although all the absolute zeta-potential values under the NaCl concentration of 100 mM were smaller than the critical aggregation values (Fig. 2-2), the pH-dependent aggregation did not occurred at pH 4.0 and 4.5 and was rather prevented at pH 5.0 and 5.5 (Fig. 2-1). Chen & Ono (2010) also reported similar phenomena that NaCl-added purified OB dispersions were stable against gravitational floating even nearby the pI. These results suggest that NaCl addition enhances solubility of the surface oleosins via the salting-in effect to inhibit aggregation of OBs formed by hydrophobic and electrostatic interactions.

3.2 Interfacial properties of soybean OBs under the various aqueous conditions

3.2.1 Dynamic interfacial tension analysis

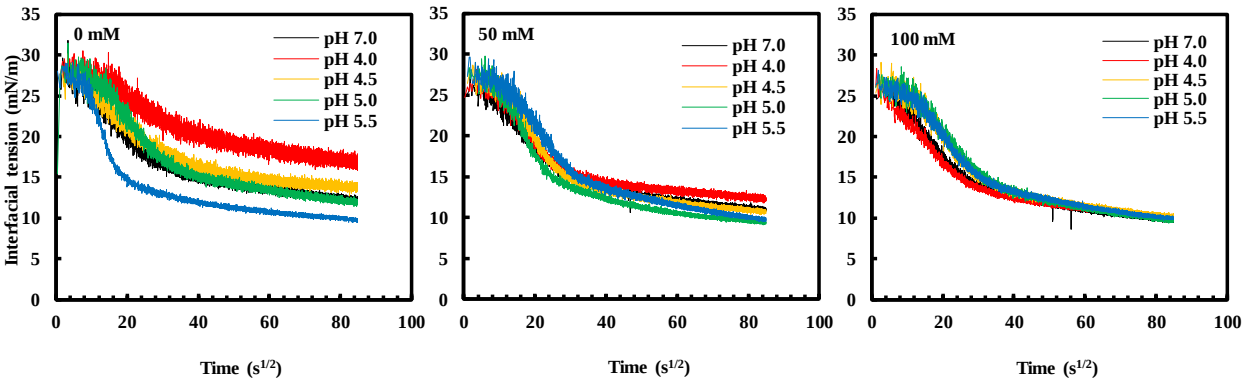

Fig. 2-3 Dynamic interfacial tension between OB dispersions and purified soybean oil under various pH values (4.0, 4.5, 5.0, 5.5, 7.0) and NaCl concentrations (0, 50, and 100 mM).

Although it is widely accepted that critical factors that affect adsorption kinetics of simple proteins are diffusion rate, molecular flexibility, and surface hydrophobicity, etc., that of colloidal particles like OBs were unknown. To clarify how the colloidal properties of OBs affect the adsorption behavior that is necessary to consider the emulsifying ability, dynamic oil-water interfacial tension measurements were carried out under the various acidic pH and salt concentration conditions. Fig. 2-3 shows time-dependent interfacial tension at the oil-water interface of OBs in the various pH buffer solutions containing 0 mM (left), 50 mM (center), and 100 mM (right) of NaCl, respectively. The interfacial tension totally decreased in a time-dependent manner under all the conditions, indicating that OBs are essentially surface-active regardless of the aqueous conditions, whereas pH-dependent variation of the interfacial tension decrease was largest at the lowest NaCl concentration (0 mM) compared with at the higher NaCl concentrations, whilst at the lowest NaCl concentration the samples at pH 4.0 and 5.5 particularly showed clearly slower and faster adsorption than those at the other pH values, respectively. The possible mechanisms at pH 4.0 under the lowest NaCl concentration is that electrostatic barrier caused by already-adsorbed and un-adsorbed OBs which possess

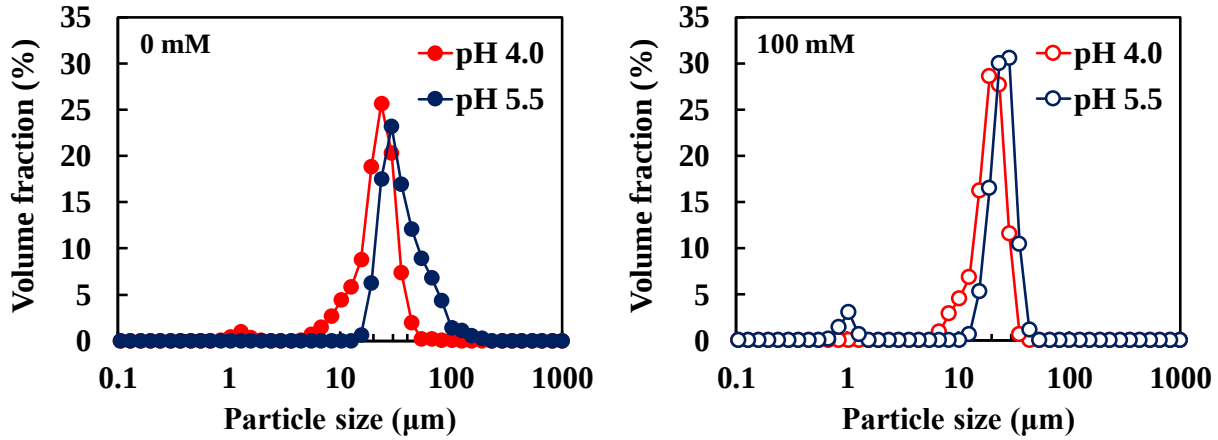

Fig. 2-4 Particle size distributions of OB-stabilized emulsions prepared under various pH values (4.0 and 5.5) and NaCl concentrations (0 and 100 mM), respectively.

strongly positive charge interfered rapid adsorption to the interface (Dickinson & McClements, 1996), suggesting that this condition might possibly cause lower emulsifying ability or physical stability of obtained emulsions. On the other hand, in the medium at pH 5.5 containing 0 mM NaCl, OBs severely aggregated to form large particles, normally leading to rather slower adsorption owing to slower diffusion and lower effective particle number, though this cannot explain the obtained result. The author supposes that some attractive forces like van der Waals forces between already-adsorbed and un-adsorbed OB aggregates might promote adsorption of OBs, since the van der Waals forces is stronger when the size of approaching particles increases.

3.3 Emulsifying properties

3.3.1 Emulsifying activity

Since the adsorption behavior of OBs at pH 4.0 and 5.5 were particularly different from that at the other pH conditions and also highly susceptible to salt addition, the author focused on the

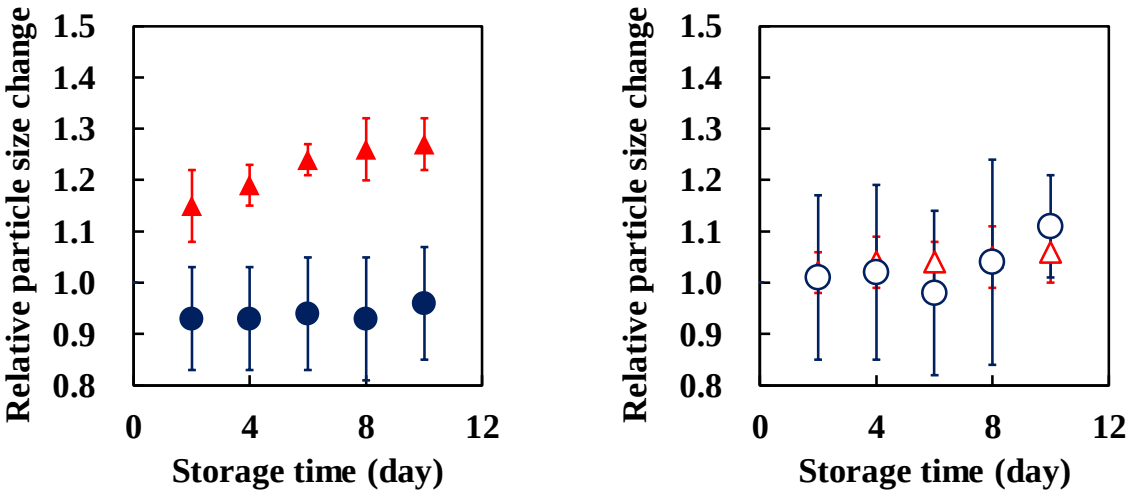

Fig. 2-5 Relative particle size changes of OB-stabilized emulsions prepared under various pH values (4.0 and 5.5) and NaCl concentrations (0 and 100 mM) during storage for 10 days. Measurements were carried out in the presence of SDS.

two pH values (pH 4.0 and pH 5.5) and two NaCl concentrations (0 mM and 100 mM), espectively, and prepared O/W emulsions using the OB dispersions to reveal combinational effects of acids and salts in the following experiments for the emulsifying properties of OBs. Fig. 2-4 illustrates the particle size distributions of OB-stabilized emulsions measured just after emulsification without SDS since SDS addition did not significantly affected the distributions. For all the prepared emulsions, the size distribution of emulsified oil droplets is almost monomodal with a slight small-sized fraction probably attributed to un-adsorbed OBs, proving that OBs have emulsifying ability even in the presence of acids and salts.

When the NaCl concentration was 0 mM, the emulsions prepared at pH 5.5 seemed to include larger oil droplets than several tens of micrometer compared to the emulsions prepared at pH 4.0. This contradictory result to the fastest interfacial adsorption rates at pH 5.5 observed in the interfacial tension measurements probably due to insufficient repulsive forces between temporarily-created oil droplets for preventing re-coalescence during emulsification or

inadequate effective concentration of aggregated OBs for covering newly-created oil droplet surfaces. On the contrary, the oil droplet size distributions of the emulsions prepared at pH 4.0 and 5.5 were almost the same under the NaCl concentration of 100 mM, suggesting that well-solubilized/dispersed OBs under the relatively higher NaCl concentration lead to improved emulsifying activity especially at pH 5.5.

3.3.2 Emulsion stability against droplet flocculation and coalescence

In order to evaluate the kinetic stability of the obtained emulsions at pH 4.0 and 5.5 containing 0 mM and 100 mM NaCl, periodical particle size measurements were performed for 10 days with/without SDS. For all the samples, the obtained emulsions seemed to involve only weak flocculation that can be easily dissociated during the storage tests, because the size distributions measured with/without SDS were not significantly different.

Fig. 2-5 depicts the relative time-dependent mean particle size changes of the samples measured in the presence of SDS. At the NaCl concentration of 0 mM, the relative particle size of the OB-stabilized emulsions prepared at pH 4.0 gradually increased, while that of the emulsions prepared at pH 5.5 did not significantly change. As the measurements were carried out with SDS, the relative size increase was attributed to oil droplet coalescence, which could possibly result from less dense packing of strongly-charged OBs at the droplet surfaces and consequently vulnerability against mechanical stress. The instability against oil droplet coalescence was not observed for the emulsions containing 100 mM NaCl even at pH 4.0, suggesting that screening of strongly-charged OBs at pH 4.0 can improve resistance against emulsion oil droplet coalescence via enabling sufficient adsorption on the droplet surfaces.

4. References

Chen, Y. & Ono, T. (2010). Simple Extraction Method of Non-allergenic Intact Soybean Oil Bodies That Are Thermally Stable in an Aqueous Medium. Journal of Agricultural and Food Chemistry, 58 (12), 7402–7407.

Dickinson, E. & McClements, D. J. (1996) Advances in Food Colloids 1st edition, Ch. 2, Chapman & Hall

Hatta, H., Hagi, T., & Hirano, K. (1997) Hen Eggs: their basic and applied science (eds Ymamoto, T., Juneja, L. R., Hatta, H., & Kim, M.) Ch. 8. CRC Press.

Huang, A. H. C. (1992). Oil Bodies and Oleosins in Seeds. Annual Review of Plant Physiology and Plant Molecular Biology, 43 (1), 177–200.

Ishii, T., Matsumiya,K., Nambu, Y., Samoto, M., Yanagisawa, M., & Matsumura, Y. (2017) Interfacial and emulsifying properties of crude and purified soybean oil bodies. Food Structure, 12, 64–72.

Kato, N. & Shibasaki, I. (1975). Comparison of antimicrobial activities of fatty acids and their esters. Journal of Fermentation Technology 53, 793-801.

McClements, D. J. (ed) Food Emulsions: principles, practices, and techniques 3rd edn (CRC Press, 2016).

Pimentel, D. & Pimentel, M. Sustainability of meat-based and plant-based diets and the environment. Am. J. Clin. Nutr. 78 (Suppl), 660S–663S (2003).

Walstra, P. (ed) Physical Chemistry of Foods. (Marcel Dekker Inc., 2003).

Chapter 3:

Microgelation imparts emulsifying ability to surface-inactive polysaccharides—bottom-up vs top-down approaches

1. Introduction

Many food products such as dressings, coffee creams, and white sauces exist as an oil-in-water (O/W) emulsion where small oil droplets are dispersed in an aqueous continuous phase (McClements, 2016). These oil droplets are mainly stabilized by surface-active biopolymers like milk and egg yolk proteins due to their high emulsifying ability occasionally together with small-molecule surfactants for food production (van Aken, 2004; Das & Kinsella, 1990), whilst such animal proteins often require much higher energy input to be produced than plant resources; for example, the required fossil fuel for 1 kcal of the animal and plant protein resources are 25 kcal and 2.2 kcal, respectively (Pimentel & Pimentel, 2003). In addition to this, the major origins of food proteins, e.g. milk, egg, wheat, and soybean, are widely recognized as allergens that need special attentions according to the Codex Committee on Food Labelling (FAO & WHO, 2001; Hefle, Nordlee, & Taylor, 1996). To avoid the allergic reactions, a lot of low-allergenicity food products such as gluten-free breads and noodles have been extensively developed especially for wheat flour products, often combined with polysaccharide-based food hydrocolloids to improve their textual quality (Houben, Höchstötter, & Becker, 2012; Toufeili et al., 1994; Marti & Pagani, 2013; Heo, Jeon, & Lee, 2014). Such low-allergenic polysaccharides originated from plants and microorganisms are eco-friendly as well, but they are not applied enough for food emulsions as an effective emulsifying agent.

Food emulsions are thermodynamically unstable systems and tend to destabilize via physical processes such as creaming, flocculation, and coalescence during transportation and in

their shelf life. The emulsifying agents applied to formation of the system are at the same time required to delay progress of these phenomena once oil and water are emulsified. Whereas small molecule emulsifiers adsorb to the oil-water interface to efficiently stabilize the system to oil droplet coalescence throughout the Gibbs-Marangoni effects (McClements, 2016; Walstra, 2003), macromolecules like proteins form elastic layers on the oil droplet surfaces during emulsification processes to provide the effective steric and electrostatic effects responsible for stability against coalescence (McClements, 2016; Dickinson, 2003). Despite these favorable properties of proteins to stabilize emulsions, the adsorbed proteins are intrinsically highly susceptible to pH value change, salt addition, and processing such as heat and freeze-thaw treatments (McClements, 2016; Fustier, Taherian, & Ramaswamy, 2010), and therefore they are often additionally covered with oppositely charged polysaccharides such as pectin, soluble soybean polysaccharide (SSPS), and carrageenan (Surh, Decker, & McClements, 2006; Mun, Cho, Decker, & McClements, 2008; Wu et al., 2012; Tran & Rousseau, 2013). Although many kinds of polysaccharides play a major role in stabilizing the interface between oil and water particularly in combination with proteins, they are not usually used for food emulsions as a sole emulsifying agent because typical hydrophilic polysaccharide molecules are surface inactive in principle unless they include protein moieties responsible for emulsifying ability like gum arabic and SSPS for emulsions designed as flavor products (McClements, 2016; Dickinson, 2003; Matsumura, Satake, Egami, & Mori, 2000; Yoshii et al., 2001; Nakamura, Yoshida, Maeda, & Corredig, 2006).

Historically, polysaccharides have been commonly utilized as a thickening agent for various food products in the food industry, e.g. locust bean gum and xanthan gum are often added into sauces and dressings, where the hydroxyl groups of polysaccharide molecules attractively interact with water molecules via hydrogen bonding to increase friction between the

molecules leading to viscous characteristics of the solution. Amongst the polysaccharides, agar, curdlan, gellan gum etc. can act as a gelling agent to form a macrogel under appropriate conditions by intermolecular interactions through association of helical domains and co-formation of helices (Armisén & Galatas, 2009; Sworn, 2009; Nishinari, Zhang, & Funami, 2009). In the last decade, polysaccharide-based microgels were developed as a delivering agent of drugs to enclose bioactive compounds for controlled releases (Coviello, Matricardi, Marianecci, & Alhaique, 2007; Oh, Drumright, Siegwart, & Matyjaszewski, 2008). On the other hand, macromolecule-based microgels, not regarding polysaccharides, have been increasingly gaining much attention as a novel class of emulsifying agents to obtain stable emulsion systems. The porous and soft microgel-stabilized emulsions referred to as Mickering emulsions (Schmidt, Liu, Rütten, Phan, Möller, & Richtering, 2011), a recently proposed scientific technical term, whose properties were found to be different from Pickering ones were initially prepared with poly(*N*-isopropylacrylamide), a synthesized surface-active macromolecule (Ngai, Behrens, & Auweter, 2005). The gel particles adsorbed on the oil droplet surfaces form relatively thick interfacial layers between the oil-water interface to introduce enhanced stability of the emulsions. More recently, edible microgels were successfully fabricated from food-grade materials such as whey and soy proteins (Destribats, Rouvet, Gehin-Delval, Schmitt, & Binks, 2014; Dickinson, 2015; Matsumiya & Murray, 2016). In this context, the author conceived of an idea that conversion of ordinary states to insoluble microgels effectively imparts emulsifying ability to less surface-active polysaccharides.

The objective of this work is to study effects of microgelation on the emulsifying ability of polysaccharides that have been rarely applied for stand-alone emulsification of food grade oils. Agar, curdlan, and gellan gum which contain few protein moieties and are widely recognized as gelling agents with different sugar units were chosen as the materials for the

preparation of microgels. The fabricated microgel particles suspended in an aqueous phase were characterized by colloidal and rheological analyses and then homogenized with soybean oils to create microgel-based Mickering emulsions. They were subjected to particle size and zeta-potential measurements, and visual and microscopic observations to evaluate emulsifying ability of microgels made from polysaccharides, followed by subsequent emulsion stability tests during several months. Microgels produced via build-up or break-down approaches were directly compared to elucidate the impact of fabrication processes on the physical stability of emulsions.

2. Materials & Methods

2.1. Materials

Agar, curdlan, and gellan gum were purchased from FUJIFILM Wako Pure Chemical Corporation, Osaka, Japan. The typical average molecular weight of agarose and agaropectin (components of agar), curdlan, gellan gum is about 100 <, < 20, 66–680, and 250–490 kDa, respectively.[21,23,43,44] Soybean oil was also obtained from the same company. Oil red O, Nile Red, and Nile Blue A were bought from MilliporeSigma, Burlington, MA, USA. Sodium 9-anilino-1-naphthalenesulfonate (ANS-Na) was acquired from Tokyo Chemical Industry Co., Ltd., Tokyo, Japan. All other general chemicals were of analytical grade. Deionized water was used for preparation of all samples and aqueous solutions.

2.2. Sample preparation

2.2.1. Preparation of microgel suspensions

Building-up methods

Agar powder (0.125 g) was dispersed to deionized water and heated at 95°C for 30 min to obtain 100 g of the solutions. The solution was cooled in a water bath at 25°C for 30 min, stirring at 550 rpm by a magnetic stirrer to prevent sedimentation and partial macroscopic gelation during this process. Curdlan powder was mixed with deionized water by the high-speed blender, followed by the deaeration for 10 min. The dispersion (100g, 0.125 wt%) was incubated in a water bath first at 95°C for 30 min and subsequently at 25°C for 30 min, stirred by the stirrer at 550 rpm during both the heating and cooling processes. Gellan gum powder (0.125 g) was dissolved to deionized water at 95°C for 30 min. The solution (95 g) was mixed with 5 g of 10 mM calcium chloride solution, and then stirred at 550 rpm by the stirrer for 30 min at 25°C. These samples prepared via the building-up processes were referred to as

BU. The pH value of all the samples was at around 6.0 with a maximum variation of 0.3.

Breaking-down methods

Macrogels made from agar, curdlan, and gellan gum were prepared in different ways as follows. For agar macrogels, agar powder was mixed with deionized water by a magnetic stirrer at 550 rpm for 10 min to obtain 1.0 wt% of agar suspensions. The suspension (100 g) was heated in a water bath at 95°C for 30 min to obtain an agar solution and subsequently cooled in another water bath at 25°C for 30 min to achieve a cold-set macrogel formation. For preparing curdlan macrogels, 1.0 g of curdlan powder was homogenized with 39 g of deionized water by a high-speed blender (Physcotron, Microtec co., ltd, Chiba, Japan) with NS-10 shaft at 20,000 rpm for 3 min at room temperature. The dispersion was deaerated using a vacuum pump for 10 min and subsequently mixed with 60 g of additional hot water (95°C), followed by an incubation in a water bath at 95°C for 30 min to ensure heat-set gelation (Nishinari et al., 2009). The obtained macrogel was cooled down to room temperature in another water bath (25°C, 30 min). For gellan gum, 1 g of gellan gum powder was dispersed in 79 g of deionized water and incubated at 95°C for 30 min to obtain a gellan gum solution. The solution was mixed with 20 g of a 10 mM calcium chloride solution and placed in a water bath at 25°C for 30 min to set an ion-induced macrogel.

Each macrogel was roughly broken into small pieces by a spatula and mixed with additional deionized water to obtain 400 g of a macrogel suspension, and subjected to homogenization by the high-speed blender with NS-20 shaft at 15,000 rpm for 1 min to obtain breaking-down coarse microgel (BD-C) suspensions. The BD-C suspensions were further processed through a high-pressure homogenizer (Star Burst Mini, Sugino machine limited, Toyama, Japan) at 80 MPa or 240 MPa to collect fine microgel suspensions. These suspensions

were defined as breaking-down samples with various high-pressure treatments, i.e. BD-80 and BD-240. All the microgel suspensions were immediately twice diluted with deionized water to achieve the final polysaccharide concentration of 0.125 wt%. The pH value of all the BD-C, BD-80, and BD-240 samples was also at around 6.0 with a maximum variation of 0.3.

2.2.2. Emulsion preparation

The microgel suspensions (40 g) were mixed with soybean oils (10 g) in plastic bottles by the high-speed blender with NS-20 shaft (15,000 rpm, 1 min), and the resultant coarse emulsions were processed in an ice-water bath by an ultrasonic homogenizer (Q700 Sonicator, Qsonica, L.L.C, Newtown, CT, USA) with a 1/2 inch probe at an amplitude of 30% for 1 min to make fine microgel-based emulsions. Control emulsions were also prepared by the following polysaccharide solutions without the gelation processes. Agar solutions (0.125 wt%) melted at 95°C were incubated in a water bath at 60°C ensuring solubilized states (Armisén & Galatas, 2009), and then homogenized with soybean oils via the same homogenization processes at a weight ratio of 1:4 in a bottle incubated in the water bath at 60°C. The obtained emulsions were kept at 60°C to prevent gelation of agar (Armisén & Galatas, 2009). Curdlan (0.125 wt%) was dissolved into a 0.2 M sodium hydroxide solution at about pH 13.0 and homogenized with soybean oils as described above. Gellan gum (0.125 wt%) was solubilized in distilled water without any additional salts at 95°C and cooled down to 25°C in a water bath, and then homogenized in the same way. Visual observation for all the emulsions was carried out for 24 h to confirm free oils released from the emulsions.

2.3. Cryo-scanning electron microscopy (Cryo-SEM)

The microgel suspensions and microgel-stabilized emulsions were observed by a scanning

electron microscope (SU8230, Hitachi High-Technologies Corporation, Tokyo, Japan) equipped with a cryogenic unit (Alto2500, Gatan UK, Abingdon, Oxfordshire, UK). The samples were filled into two metal hollow rivets with the edges contacted, and rapidly frozen in nitrogen slush. The lower part of the rivets was fixed on a metal stage and then inserted into the loading chamber of the microscope, and subsequently split into the original two parts to remove the upper one. The cleaved surface of the lower rivet was observed after appropriate sublimation at -120°C.

2.4. Particle size analysis

Three methods were applied for particle size analysis of microgel suspensions. The particle size distribution of microgel suspensions was first analyzed by dynamic light scattering (DLS) at 25°C (Nicomp 370 submicron particle size analyzer, Particle Sizing System, Inc., Port Richey, FL, USA) using the solid particle mode and Nicomp distribution analysis mode assuming multi-modal distributions.

The particle size of the microgel suspensions was also measured using a laser-diffraction particle size analyzer (SALD 2200, Shimadzu Corporation, Kyoto, Japan) with the refractive index of $1.45 - 0.00i$.

Next, the particle size distribution of microgel suspensions was determined using a Coulter counter particle size analyzer (Multisizer 4e, Beckman Coulter, Brea, CA, USA). An aliquot of the sample suspensions containing 0.125 wt% of polysaccharides were dispersed into a 0.9 wt% sodium chloride solution in a dispersing chamber with an assistance of 0.2 wt% SDS that prevent possible aggregation. The volume-based particle diameter is individually calculated from conductivity change between the electrodes in an aperture unit. A 100 μm aperture unit with the detection range of from 2 to 60 μm was used, and the particle size distribution was

obtained from approximately 50,000 particles. The $d_{4,3}$, mode, d_{10}, d_{50}, and d_{90} values were obtained from the distribution, and SPAN was calculated according to the following equation (Seemann, Hauff, Schultze-Mosgau, Lehmann, & Reszka, 2002):

$$\text{SPAN} = \frac{d_{90} - d_{10}}{d_{50}}$$

For the gellan gum microgel dispersions, the fourth method, i.e., size exclusion chromatography coupled with multi-angle light scattering (SEC-MALS) was applied for determining particle size distribution. The gellan gum microgel dispersions (0.25 wt%) were filtrated through a syringe-driven disposable filter unit with a polypropylene membrane with 2 μm pore (Puradisc™ 25 GD2, Whatman®, Whatman Inc., Marlborough, MA, USA). The filtrates (50 μl) were injected and separated by a size exclusion chromatograph (1260 Infinity, Agilent Technologies, Santa Clara, CA, USA) through three columns (OHpak SB-G 6B guard column, OHpak SB-806 HQ, and OHpak SB-805 HQ, Shodex™, Showa Denko K.K., Tokyo, Japan) at the flow rate of 0.5 ml/min. The separated samples were subsequently detected by a UV absorbance detector (1260 VWD, Agilent Technologies, Santa Clara, CA, USA) at 258 nm, a differential refractive index detector (Optilab T-rEX, Wyatt Technology Corporation, Santa Barbara, CA, USA) with dn/dc value of 0.155 ml/mg (Milas, Shi, & Rinaudo, 1990), and multiple-light scattering detectors (DAWN HELEOS-II, Wyatt Technology Corporation, Santa Barbara, CA, USA). The obtained data were processed using an attached software (ASTRA Ver. 6.1) to calculate radius of gyration of particles and its weight-based distribution. The concentration of samples was assumed to be 2.5 mg/ml, and a 0.1 M $NaNO_3$ solution was used as an eluent. All the analysis were carried out at 25°C.

The microgel-based emulsions were subjected to particle size analysis using the laser-diffraction particle size analyzer in the same way as the measurements of microgels.

Volume weighted mean particle size ($d_{4,3}$) was calculated for presentation.

2.5. Zeta-potential measurements

The zeta-potential of microgel particles and emulsion oil droplets was measured using a laser-Doppler zeta-potential analyzer (ELS-Z1, Otsuka electronics co. ltd., Osaka, Japan). The microgel suspensions and microgel-based emulsions were several times diluted with deionized water to obtain appropriate light scattering intensity when required. The measurements were performed at 25°C and repeated 3 times for each sample.

2.6. Rheological measurements

Rotational viscometry

Apparent shear viscosity of the microgel dispersions was measured using a rotational rheometer (Rheosol G3000, UBM, Kyoto, Japan) attached with a coaxial-double-cylinder probe. An aliquot (3.0 ml) of samples incubated in a water bath at 25°C was poured into the lower outer hollow cylinder (ϕ = 17.99 mm), and subsequently the cylindrical part of the upper inner cylinder (ϕ = 15.99 mm, h = 26.04 mm) was completely immersed into the sample to adjust the gap between these cylinders' bottoms to 6 mm. The lower outer cylinder was rotated and the shear rate dependent changes of the shear stress were measured within a range from 0.0096 s^{-1} to 9.97 s^{-1} at 25°C. Apparent viscosity values were calculated using obtained shear stress (σ) and shear rate ($\dot{\gamma}$) values based on the following equation (Hunter, 2001):

$$\text{Apparent viscosity} = \frac{\sigma}{\dot{\gamma}}$$

Vibration vicometry

The viscosity measurement for microgel suspensions was carried out using a tuning fork vibro rheometer (RV-10000A, A&D company, limited, Tokyo, Japan). A 10 ml of sample was subjected to the measurements with 0.4 mm of amplitude for 3 min to collect static viscosity (V_s) converted from the vibration resistance. The viscosity of the samples was calculated from the initial static viscosity values by the following equation:

$$\text{Viscosity} = \frac{V_s}{d}$$

where d is density of the sample. The density of microgel suspensions and emulsions were assumed to be 0.997 g/cm^3 and 0.980 g/cm^3, respectively, based on that of water (0.997 g/cm^3) and soybean oils (0.917 g/cm^3) at 25°C. All the measurements were performed at 25.0 ± 0.5°C, and each sample was measured 3 times.

2.7 Interfacial tension measurements

To precisely evaluate interfacial activity of the prepared polysaccharide microgels, the author first conducted soybean oil purification to remove slightly-existing surface active polar compounds such as fatty acids and mono- and di-acylglycerols from the oil according to the previous research by Murphy, Farkas, & Jones (2016). The interfacial tension between the aqueous microgel dispersions and the purified oil was measured based on the pendant drop technique using a drop tensiometer (Tracker, Teclis Scientific, Tassin la demi lune, Rhône, France). The aqueous microgel dispersions were diluted 10 times with deionized water and filled into a glass call (25 ml). The tip of a rising-type needle attached to a syringe filled with the purified oil was immersed into the aqueous microgel dispersion, followed by creation of a rising oil drop into the aqueous phase. The surface area of the created oil drop was controlled to 30 mm2 and the interfacial tension were time-dependently calculated based on the density of

two phases (0.997 g/cm3 and 0.917 g/cm3 for water and oil, respectively) and the drop shape images captured by a CCD camera. Measurements were carried out at 25°C for 30 min.

2.8. Determination of surface hydrophobicity

The surface hydrophobicity of microgles was determined using a fluorescence probe, ANS-Na (Kato & Nakai, 1980). The microgel dispersions (0.1 – 0.5 wt% polysaccharides) were mixed with an aliquot (50 μl) of a 8 mM ANS-Na solution, and the mixture was subsequently incubated in a water bath at 25°C for 10 min, followed by fluorescence measurements by a spectrofluorometer (FP-8300, JASCO corporation, Tokyo, Japan) with the excitation and emission wave lengths of 390 nm and 470 nm, respectively. A slope of the biplot of the polysaccharide concentration and arbitrary fluorescence intensity was used as a surface hydrophobicity index.

2.9. Evaluation of physical stability of microgel-stabilized emulsions

2.9.1. Observation of creaming behavior

The emulsions were mixed with an aliquot of sodium azide solution to achieve the final concentration of approximately 0.02 wt% and filled into 30 ml of vials immediately after the preparation. The vials were placed on a flat table at 20°C for 24 h, and the creaming behavior was observed every 30 min. The creaming index was calculated using the following equation:

$$\text{Creaming index (\%)} = \frac{H_s}{H_t}$$

where H_t and H_s are total height and serum layer height of the emulsions, respectively. The initial creaming rate of the microgel-stabilized emulsions was also determined by linear

correlation of the creaming rate plots within the first 2 h. The obtained creaming rate values were compared with theoretical creaming rate calculated by the following equations (McClements, 2016):

$$V_0 = \frac{D^2(\rho_w - \rho_o)g}{18\eta}$$

where V_0 is the creaming velocity calculated by Stoke equation, D is the oil droplet diameter, ρ_w and ρ_o are the density of water and oil (0.997 and 0.917, respectively), and g is the acceleration due to gravity. The obtained viscosity values of the emulsions were used as η in this study.

2.9.2. Evaluation of flocculation and coalescence

The microgel-stabilized emulsions containing 0.02 wt% of sodium azide were stored in an incubator at 25°C for 8 weeks and subjected to periodical particle size measurements every week. The emulsion was gently mixed by turning the tube upside down 10 times and diluted with an equal volume of water with/without 2 wt% SDS before measurements (Gelin, Poyen, Courthaudon, Le Meste, & Lorient, 1994).

2.9.3. Quantification of accelerated oil phase separation

The emulsions (10 ml) were centrifuged at 20,000×g for 30 min at 25°C. The forcibly destabilized free oils were quantified according to Palanuwech, Potineni, Roberts, & Couplan (2003). Briefly, after the centrifugation, bulk oils at the top released from the emulsion systems were mixed with 2 g of additional soybean oils containing 0.002 wt% of Oil Red O, followed by a centrifugation under the same conditions to completely remove contaminants. The absorbance of colored oils at 517 nm was measured. The mass fraction of released free oils, ϕ_d, was calculated using the following equation (Palanuwech et al., 2003):

$$\phi_d = \frac{m_o(a - 1)}{m_e \phi_e}$$

where ϕ_e is the mass fractions of oils in the original emulsion, m_o and m_e are respective weight of the added Oil Red O solutions and the emulsions, and a is absorbance measured at 517 nm, respectively.

2.10. Confocal laser scanning microscopy (CLSM)

Agar and curdlan were stained by dissolving Nile Blue A and ANS-Na into the microgel suspensions to achieve the final concentration of 0.1 wt% and 0.5 wt%, respectively. Oils were dyed with Nile Red (0.1 wt%) prior to emulsification. The sample was observed without any dilutions using a confocal laser scanning microscope (FV1000, Olympus Corporation, Tokyo, Japan). The excitation and emission wavelengths were 635 nm and 647 nm for Nile Blue A, 405 nm and 422 nm for ANS-Na, and 473 nm and 520 nm for Nile Red, respectively.

2.11. Statistical analysis

All samples were prepared at least 3 times. The obtained values were reported as means ± standard deviations based on triplicate experiments. Representative images were shown for microscopic and visual observations. All statistical analyses were performed by Microsoft Excel version 2016. The statistical significance among the differently prepared microgels was tested by analysis of variance ($p = 0.05$).

3. Results & discussion

3.1 Colloidal properties of microgel particles

Colloidal properties of dispersed microgel particles were studied because these properties definitely affect emulsifying ability of particles (Destribats et al., 2014). the author prepared microgels from 3 types of polysaccharides via the gel formation under diluted conditions as a building-up approach (BU) and the mechanical breakage of macrogels as a breaking-down approach (BD-C, BD-80, and ND-240). Microstructure, size, and zeta-potential of the particles and viscosity of the overall dispersion systems that significantly influence physical stability of emulsions were analyzed.

As all the obtained microgel suspensions were almost transparent and difficult to observe by light microscopy, cryo-SEM was carried out to analyze microstructure of the gel particles. Fig. 3-1 depicts cryo-SEM images of the microgel suspensions captured at a magnification of ×1000. For all the agar microgel suspensions (Fig. 3-1 (a1–a4)), micro-ordered gel-like particles about 10 μm with remaining networks were found, and BU and BD-240 particles seemed to be surrounded by fibrous materials highlighted by *. For curdlan, BU and BD-C suspensions (Fig. 3-1 (b1) and (b2)) included large clusters of several tens of micrometers, whereas BD-80 and BD-240 particles (Fig. 3-1 (b3) and (b4)) were mostly smaller compared to such large clusters, meaning that the ultra-high-pressure processing efficiently broke down the curdlan macrogels. These results from the agar and curdlan samples clearly show the formation of microgel particles via both the building-up and breaking-down processes. In the gellan gum suspensions, on the other hand, fibrous networks radially expanded over the observed ice crystal fields, where micro-ordered particles were not found for all the samples prepared (Fig. 3-1 (c1–c4)). This indicates that gellan gum molecules hardly coagulated even after Ca^{2+} addition under the diluted condition in the BU preparation, while the

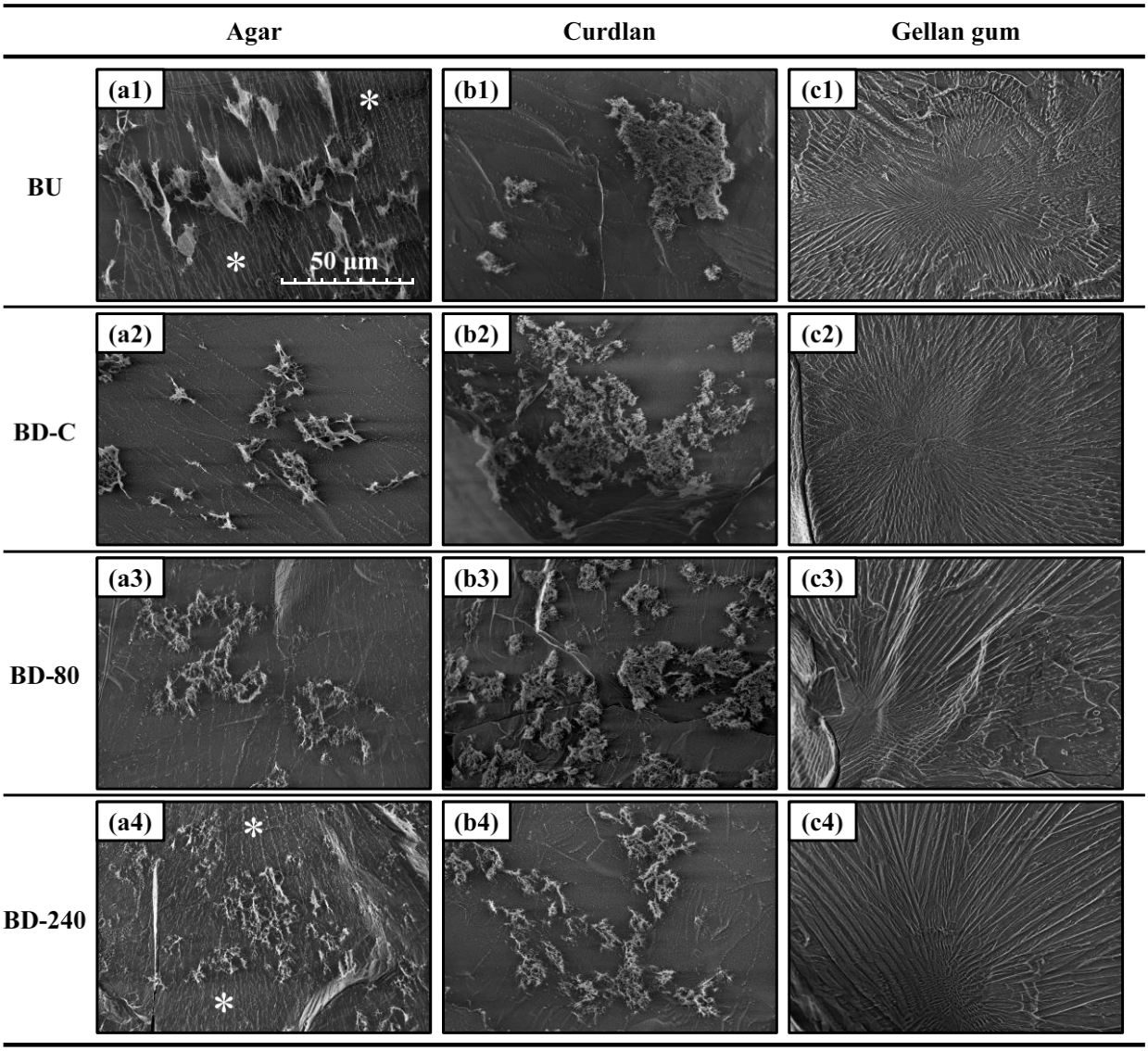

Fig. 3-1 Microstructure of the obtained microgels observed by cryo-SEM. All the sample dispersions (0.125 wt%) filled in a pared metal tube were frozen in a slash nitrogen, sublimated, and subsequently observed at -120°C. Scale of all images is the same (50 μm).

molecules that once associated by Ca^{2+} addition to form macrogels were atomized into almost soluble submicron states by the breaking-down treatments in BD-C, BD-80, and BD-240 preparations.

In order to evaluate the particle size of the agar, curdlan, and gellan gum microgels, the author carried out particle size measurements by DLS and laser-diffraction techniques.

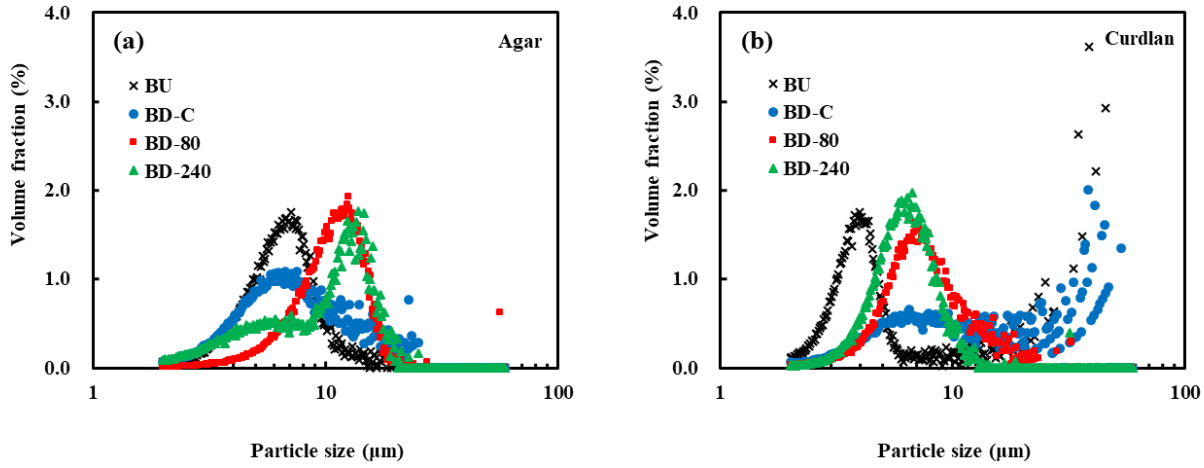

Fig. 3-2 Volume-weighted particle size distribution of (a) agar and (b) curdlan microgels measured by the Coulter principle particle size analyzer with a detection range of from 2 to 60 μm.

Table 3-1 Representative values calculated from the particle size distributions of agar and curdlan microgels (mean ± S.D., n=3).

		$d_{4,3}$ (μm)	mode (μm)	d_{10} (μm)	d_{50} (μm)	d_{90} (μm)	Span
Agar	**BU**	6.81 ± 0.53	7.50 ± 0.83	4.30 ± 0.63	6.86 ± 0.74	10.42 ± 0.42	0.91 ± 0.21
	BD-C	7.50 ± 0.16	7.07 ± 1.08	3.93 ± 0.21	7.24 ± 0.15	15.55 ± 1.38	1.60 ± 0.19
	BD-80	10.54 ± 0.33	12.48 ± 0.10	6.35 ± 0.84	11.13 ± 0.31	15.44 ± 0.23	0.82 ± 0.09
	BD-240	9.27 ± 0.42	12.95 ± 1.50	4.32 ± 0.80	10.56 ± 0.58	16.07 ± 0.54	1.11 ± 0.05
Curdlan	**BU**	7.05 ± 0.17	4.04 ± 0.03	3.04 ± 0.04	4.49 ± 0.07	38.85 ± 2.61	7.97 ± 0.49
	BD-C	12.24 ± 1.45	5.88 ± 1.12	3.68 ± 0.90	9.38 ± 3.20	39.13 ± 4.38	4.01 ± 1.02
	BD-80	7.31 ± 0.30	6.90 ± 0.05	4.47 ± 0.24	7.15 ± 0.24	12.72 ± 0.76	1.15 ± 0.07
	BD-240	5.99 ± 0.28	6.24 ± 0.44	3.99 ± 0.33	6.01 ± 0.24	8.72 ± 0.18	0.79 ± 0.06

However, presumably due to insufficient low scattering light intensity of the transparent polysaccharide microgel particles, any reproducible and reliable values without multiple light

scattering were not successfully obtained for almost all the samples. To avoid such a problem, another non-light dependent method based on Coulter principle with electrolytes was applied for the sample analyses.

Fig. 3-2 (a) and (b) show volume-based particle size distributions of the agar and curdlan microgels measured by the Coulter principle-based particle size analyzer. Representative values from the distributions are summarized in Table 3-1. The particle size distribution of BU, BD-C, and BD-80 agar microgels was monomodal, whereas that of BD-240 seemed to be bimodal (Fig. 3-2 (a)). The average size of BU and BD-C particles without the high-pressure treatments was smaller than that of BD-80 and BD-240 ones with the treatments according to the $d_{4,3}$ and mode values shown in Table 3-1. It should be noted that the average particle sizes rather increased via high-pressure processing that is usually helpful for obtaining finer particles. This unexpected contrary tendency is probably attributed to partial solubilization of agar particles by the ultra-high-pressure treatments and subsequent reorganization leading to spontaneous formation of large particles. The partial solubilization can be supported by the presence of fibrous structure observed by cryo-SEM marked with * (Fig. 3-1 (a4)) and the increased viscosity presented in the following section (Fig. 3-4 (ii-a) and (ii-d)). The Span value as an index of polydispersity obtained from the size distribution of the agar microgel particles was significantly different from each other (one way ANOVA, $p<0.05$), while there were no clear relationships between the Span values and the added shear stresses during the sample preparation (Table 3-1).

The particle size distributions of all types of the curdlan particles mostly seemed to be monomodal with almost the same size range as that of the agar particles approximately from 2 μm to 20 μm (Fig. 3-2 (b)). The BU dispersion with an averaged particle size of 4 μm included relatively larger particles > 20 μm probably originated from the water-insoluble powdered

curdlan that could not be completely dispersed to the aqueous phase by a high-speed blending of the curdlan powder. The BD-C dispersions prepared via the formation of macrogels also possessed such large particles, whereas the particles of approximately 6 μm with a broader monomodal distribution were predominantly observed. The large particles observed for the BU and BD-C dispersions extinguished through the high-pressure processing applied for the BD-80 and BD-240 samples, meaning that most of them were successfully atomized into micron-ordered particles by the processing. The resultant distributions obtained from the BD-80 and BD-240 were both monomodal with the mode values of 6.90 μm and 6.24 μm, respectively. On the contrary to the Span values calculated from particle size distributions of the agar microgels, the values of the curdlan microgels decreased depending on the increase of the added shear stresses during the breaking-down treatments.

On the other hand, due to the limited detection range (2 - 60 μm) of the used aperture unit, it was difficult to determine the particle size distributions of the gellan gum microgels, indicating that the particle size of most populations were below 2 μm. In fact, the gellan gum microgels easily passed through a filter with 2 μm pores without any excessive pressure and were difficult to find in the cryo-SEM images (Fig. 3-1 (c1–c4)). To analyze the particle size distribution of gellan gum microgels, SEC-MALS was further performed for the filtrated gellan gum dispersions. Fig. 3-3 shows differential particle size distributions of radius of gyration obtained from the SEC-MALS for the gellan gum microgle dispersions. All the size distributions looked like the normal distribution, different from the log-normal distribution typically observed in a volume-weighted laser diffraction particle size analysis. The predominant peaks were present between 100 nm and 130 nm for all the samples (Fig. 3-3) and the average sizes were around 100 nm (Table 3-2), clearly demonstrating that the gellan gum microgels were nano-ordered assemblies. According to Takahashi et al. (2004), the average

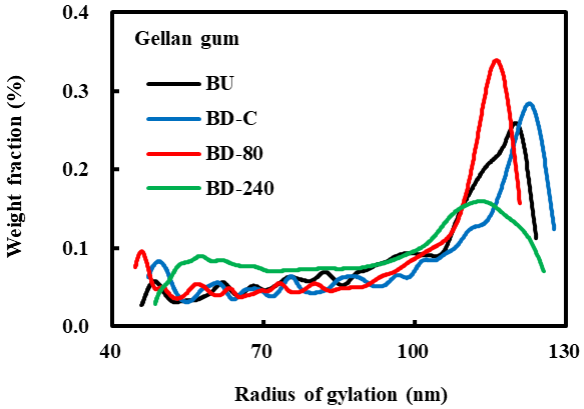

Fig. 3-3 Weight-based particle size distribution of gellan gum microgels analyzed by SEC-MALS.

Table 3-2 Mean and mode sizes of gellan gum microgels calculated from the particle size distributions (mean ± S.D., n=3).

	mean (nm)	mode (nm)
BU	85.56 ± 5.37	120.14 ± 1.89
BD-C	89.71 ± 5.15	122.00 ± 4.29
BD-80	88.05 ± 1.68	115.86 ± 6.34
BD-240	82.92 ± 2.72	112.41 ± 2.43

radius of solubilized gellan gum measured by static light scattering at 40°C were about 30 nm; therefore, the author can conclude that the author was able to prepare gellan gum microgels throughout the methods conducted in this study. This can be supported by the fact that the major peak area of particle size distributions of the BD-C gellan gum microgels obviously decreased and subsequently a novel peak appeared at around 55 nm after the high-pressure treatment at 240 MPa (BD-240), presumably due to additional dissociation between gellan gum molecules forming microgels.

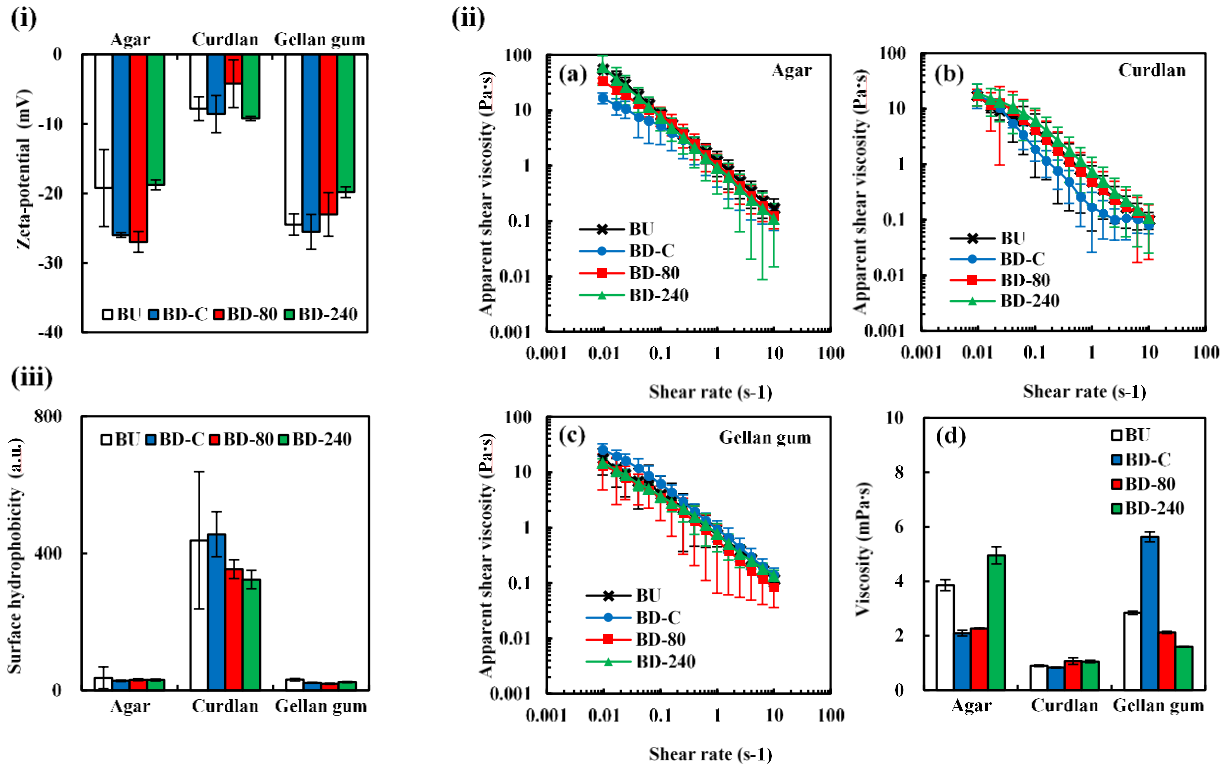

Fig. 3-4 Colloidal properties of the microgel dispersions (mean ± S.D., n=3). (i) Zeta-potential of microgel dispersions in an aqueous phase at 25°C. (ii) Viscosity of microgel dispersions. (a) - (c) Shear rate-dependent changes of apparent shear viscosity of microgel dispersions (0.125 wt%) measured using the rotational viscometer with a coaxial dual cylinder at 25°C. (d) Viscosity measured by vibration viscometer with a vibration amplitude of 0.4 mm. (iii) Surface hydrophobicity analyzed with ANS-Na. The slope of fluorescence intensity (excitation and emission wave length of 390 nm and 470 nm, respectively) vs polysaccharide concentration biplot was linearly calculated as a surface hydrophobicity index.

To estimate interactive forces of a dispersed microgel particle between other surrounding particles or the surface of added oils during the emulsification in the following process, zeta-potential of microgel particles were determined (Fig. 3-4 (i)). There was statistically significant difference between the zeta-potential values of the agar microgel particles prepared via the various types of processing (one-way ANOVA, $p<0.05$). The obtained zeta-potential values of the agar microgel particles were similar to those reported in previous

Table 3-3 Summarized values of zeta-potential, viscosity, and surface hydrophobicity analyses. The viscosity values were obtained by rotational viscometry at the low shear rate of 0.0096 s^{-1} (left) and by vibration viscometry at the high shear rate of > 10 s^{-1} with an vibration amplitude of 0.4 mm (right). All the values are expressed as mean ± S.D. (n=3).

		Zeta-potential (mV)	Viscosity low shear (Pa·s)	Viscosity high shear (mPa·s)	Surface hydrophobicity (a.u.)
Agar	BU	-19.22 ± 5.53	54.6 ± 1.3	3.85 ± 0.20	36.7 ± 32.1
	BD-C	-25.98 ± 0.33	16.8 ± 3.7	2.10 ± 0.11	28.1 ± 1.8
	BD-80	-26.97 ± 1.49	34.3 ± 3.7	2.27 ± 0.01	31.2 ± 4.3
	BD-240	-18.78 ± 0.42	62.7 ± 34.5	4.95 ± 0.31	30.5 ± 3.1
Curdlan	BU	-7.81 ± 1.71	17.2 ± 2.2	0.90 ± 0.03	437.9 ± 200.0
	BD-C	-8.57 ± 2.68	18.9 ± 8.8	0.83 ± 0.02	455.7 ± 65.4
	BD-80	-4.20 ± 3.45	16.7 ± 5.5	1.07 ± 0.12	353.9 ± 45.7
	BD-240	-9.21 ± 0.31	19.4 ± 8.2	1.05 ± 0.05	323.4 ± 27.1
Gellan gum	BU	-24.48 ± 1.54	17.8 ± 8.8	2.84 ± 0.06	31.2 ± 3.9
	BD-C	-25.53 ± 2.49	26.0 ± 6.5	5.63 ± 0.18	22.3 ± 1.3
	BD-80	-23.02 ± 3.13	13.1 ± 8.3	2.12 ± 0.04	19.2 ± 6.8
	BD-240	-19.81 ± 0.76	15.0 ± 2.4	1.60 ± 0.01	24.3 ± 1.6

studies, that is approximately -20 mV (Rocha, Souza, Magalhães, Andrade, & Gonçalves, 2014; Boral, & Bohidar, 2010). The BD-C and BD-80 particles prepared via macrogel formation indicated slightly lower zeta-potential values, which could be attributed to different structural features related to the surrounding state of sulfated groups on the surface of particles. All the absolute zeta-potential values were of about 20 mV, probably enough to generate electrically repulsive forces between particles helpful for preventing strongly-binding aggregation (Rabiey & Britten, 2009; Zhong, Fu, Peng, Zhan, & Sun, 2012). The results also suggest that the negatively-charged agar particles would not preferably access to the oil surfaces with negative charge by hydroxyl ions which are newly created during emulsification (Destribats et al., 2014; Deshiikan & Papadopoulos, 1995; Pashley, Francis, & Rzechowicz, 2008).

The zeta potential values of curdlan microgels were not significantly different among all the samples, and the absolute values of the curdlan microgel particles were totally < 10 mV and relatively smaller compared to that of the agar ones presumably because curdlan molecules mostly consist of β-glucan without any acidic groups. The low zeta-potential values generally lead to weak repulsive forces between colloidal particles, maybe explaining the presence of large granules detected in the particle size analyses of the curdlan BU and BD-C (Fig. 3-2 (b)) and suggesting that the dispersed curdlan microgel particles tend to associate to form weakly-packed flocs. During emulsification with added oils, it is expected that the curdlan microgels are able to more easily access to oil-water interfaces than the agar microgels regarding electrostatic interactions, contributing to efficient adsorption onto the newly-created oil droplet surfaces.

In the case of gellan gum, all the zeta-potential values of the microgels seemed to be independent of the processing during the microgel preparation. The zeta-potential values of the gellan gum microgels were generally similar to those of the agar microgels according to the presence of carboxyl groups (Sworn, 2009), implying that the gellan gum particles may not attractively interact with each other and with negatively-charged oil surfaces newly-created during emulsification as discussed for the agar microgels.

To shed insight into the assembly structure of polysaccharide microgel macromolecules in aqueous phases and to assess adsorption efficiency to the oil-water interfaces via diffusion process to form microgel-stabilized emulsions in the following section, viscosity of the microgel dispersions was measured using the coaxial-cylinder rotational-type viscometer suitable for flow behavior analyses and low shear rates measurements and tuning-fork vibration viscometer appropriate for low viscosity liquid as water at high shear rates (Fig. 3-4 (ii)). Since flow behavior of all the microgel dispersions were non-Newtonian and

typical shear-thinning (Fig. 3-4 (ii-a), (ii-b), and (ii-c)), the author discusses representative values at a low shear rate (0.0096 s^{-1}) and a high shear rate (vibration amplitude = 0.4 mm that is equivalent to > 10 s^{-1}) obtained from the two viscometers.

The viscosity of all the microgel dispersions at the low shear rate was extremely higher than that of water only about 0.98 mPa·s at 25°C (Fig. 3-4 (ii-a)), clearly indicating that there were some attractive interactions between the dispersed microgel particles regardless of the polysaccharide types. The viscosity of agar microgel dispersions at the low shear rate was significantly different according to the microgelation methods (one-way ANOVA, $p<0.05$) and the values were in order of BD-240 ≈ BU > BD-80 > BD-C. This tendency corresponds to possible partial dissociation states of agar macromolecules obtained from the cryo-SEM observation; i.e., the outside fibrous network of the microgel particles expanded into the surrounding aqueous phase particularly for BU and BD-240 samples (marked by * in Fig. 3-1 (a1) and (a4)). Therefore, the different viscosity values can be explained by overlapping, inter-penetrating, and entangling of polysaccharide macromolecules via the frequently-switching hydrogen bonding (Williams & Phillips, 2009).

The viscosity of curdlan microgel dispersions was not significantly different among the processing at the low shear rate (Fig. 3-4 (ii-b)). All the curdlan microgel dispersions were of relatively low viscosity to the agar dispersions at the same shear rate (Fig. 3-4 (ii-a) and (ii-b)). Throughout the cryo-SEM analyses (Fig. 3-1 (b1–b4)), the author confirmed that the curdlan microgel particles seemed to be independently dispersed without clearly observed expanding fibrous networks in the aqueous phase. These results mean that curdlan microgel particles more weakly interacted attractively with each other in water compared to agar microgels, regardless of the relatively low absolute zeta-potential values of curdlan microgels leading to particle aggregations. Similar tendencies were found for the differently treated gellan gum microgel

dispersions (Fig. 3-4 (ii-c)) and for the overall viscosity values of the gellan gum microgel dispersions in comparison with the agar dispersions (Fig. 3-4 (ii-a) and (ii-c)).

The shear viscosity values obtained by the rotational viscometer at the relatively high shear rates were inevitably accompanied with nonnegligible experimental errors due to the detection limit. the author therefore performed high shear rate vibro-viscometry and subsequently obtained viscosity values (Fig. 3-4 (ii-d)). At the high shear rate, the viscosity of agar microgel dispersions was significantly different according to the microgelation methods (one-way ANOVA, $p<0.05$) and the values were in order of BD-240 > BU > BD-80 ≈ BD-C. All the curdlan microgel dispersions were of relatively low viscosity at almost the similar level to that of water only (about 0.98 mPa·s at 25°C), and less viscous than the agar dispersions. The viscosity of gellan gum microgel dispersions was significantly different (one-way ANOVA, $p<0.05$), and it was highest for BD-C, followed by BU, BD-80, and BD-240. All these tendencies were similar to the results obtained by the high shear rate rotational viscometry

3.2 Emulsifying properties of microgel particles

Emulsifying ability

First of all, in order to examine emulsifying ability of the polysaccharides themselves, agar, curdlan, and gellan gum were dissolved into water and homogenized with soybean oils to produce soybean oil-in-water emulsions as described in Materials and Methods part. In this study, the author defined emulsifying ability as whether or not 20 wt% of soybean oils – the oil content applicable for various commercial food products – can be completely emulsified into fine oil droplets in the colloidal scale ranged between 10^{-6} and 10^{-9} m. Even though the preparation methods were intensively oriented to make the appropriate polysaccharide solution so that the temperature, pH, and ionic strength conditions were not necessarily controlled

completely, i.e., not directly comparable to the microgel dispersions, the author confirmed that the temporarily emulsified oils extensively turned into bulk states in a macroscopic scale immediately after homogenization processes (data not shown).

To reveal effects of microgelation on the emulsifying ability of the polysaccharides, the author prepared polysaccharide microgel dispersions to create microgel-based emulsions containing the same oil, followed by visual observations of initial states of the emulsions. Resultantly, all the agar and curdlan microgel-stabilized emulsions did not macroscopically separate into oil and water phases at 25°C, indicating that the agar and curdlan microgels possess high emulsifying ability worthwhile thoroughly investigating the emulsifying properties in the following section. On the other hand, the gellan gum microgel dispersions could not stabilize all the added oils in the colloidal scale with free oil layers present at the top.

Emulsifying ability is often discussed by interfacial tension measurements for classical small molecule emulsifier-stabilized emulsions, whereas the tensiometry is not necessarily applicable for particle-stabilized emulsions due to the limited capability of particles to reduce the interfacial tension between oil and water (Zhang et al., 2017). Although the adsorption schemes of soft microgels at the interface are still in arguments (Dickinson, 2015), the author confirmed that the polysaccharide microgels prepared in this study scarcely lowered the interfacial tension at the oil-water interface according to the pendant drop tensiometry (data not shown), probably indicating the tensiometry is not a useful tool for discussing emulsifying ability of the surface-inactive polysaccharide microgels.

Emulsifying ability of a surface-active molecule is generally recognized as the resultant balance of two-competently occurring coincide phenomena – formation and re-coalescence of oil droplets during emulsification process consisting of adsorption efficiency and resistance against oil droplet collisions. Adsorption efficiency related to availability of

applied shear energy depends on accessibility and diffusion rate of the surface-active molecule to the newly created oil surfaces. These molecular properties for the three kinds of microgel samples were estimated by the zeta-potential, viscosity at the high shear rate, and particle size analyses summarized in Table 3-1, 3-2, and 3-3 (based on Figs. 3-2, 3-3, and 3-4 (i) and (ii-d), respectively). As a result, the accessibility represented as zeta-potential was in order of curdlan > agar ≈ gellan gum, and the diffusion rate assessed by viscosity and particle size was curdlan > agar ≈ gellan gum and gellan gum > agar ≈ curdlan, respectively. In addition, since adhesiveness or affinity of the surface-active molecule to oil phases often represented by surface hydrophobicity could affect its adsorption efficiency, the author further evaluated the surface hydrophobicity of microgel particles using a fluorescence probe, ANS-Na. The respective obtained surface hydrophobicity index values of BU, BD-C, BD-80, and BD 240 microgel particles were 36.7 ± 32.1, 28.1 ± 1.8, 31.2 ± 4.3, and 30.5 ± 3.1 for agar, 437.9 ± 200.0, 455.7 ± 65.4, 353.9 ± 45.7, and 323.4 ± 27.1 for curdlan, and 31.2 ± 3.9, 22.3 ± 1.3, 19.2 ± 6.8, and 24.3 ± 1.6 for gellan gum (Fig. 3-4 (iii)), meaning that the adhesiveness or affinity evaluated based on surface hydrophobicity was curdlan > agar ≈ gellan gum. All these tendencies do not totally correspond to the emulsifying ability of polysaccharide microgels, that is agar ≈ curdlan > gellan gum, suggesting the adsorption efficiency that is critically important at the initial stage of emulsion formations ought not to be of decisive significance for the emulsifying ability.

It should be noted that large microgels prepared with agar and curdlan were able to stabilize all the added oils, whereas small-sized gellan gum microgels were not capable of emulsifying all the added oils. In addition to this, the free oil volume ratio to the added total oils of BU, BD-C, BD-80, and BD-240 was 20.8%, 32.3%, 54.1%, 93.2%, respectively; this is correlated to the mode values of particle size distribution of gellan gum microgels (r = -0.929).

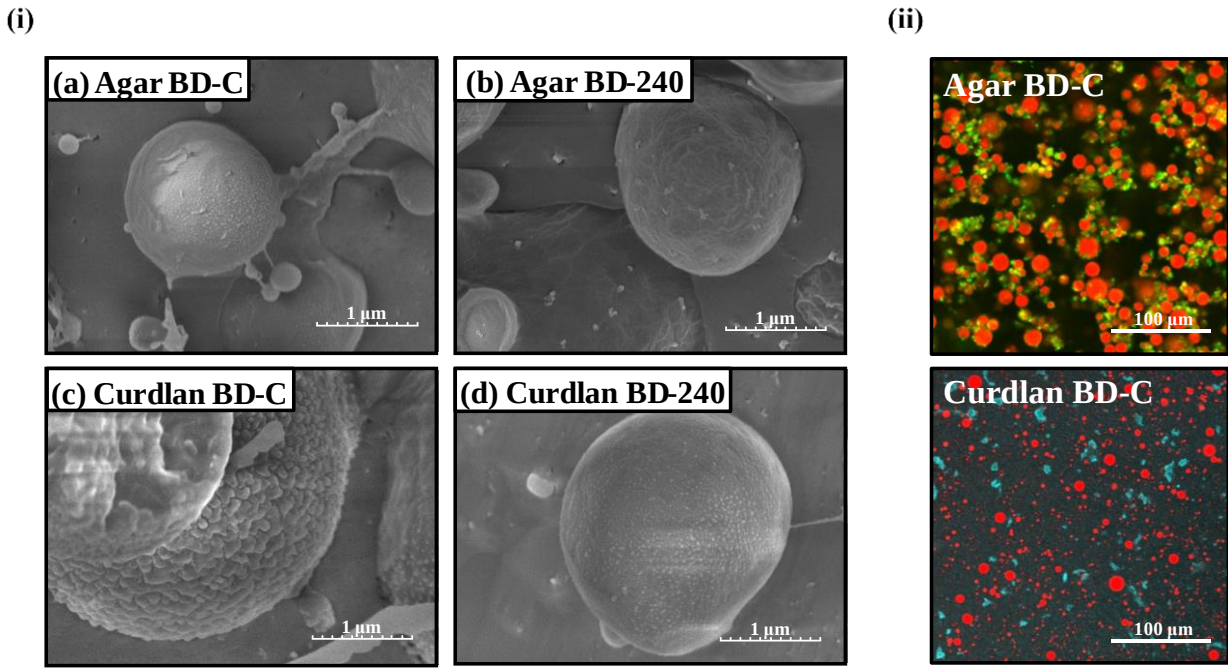

Fig. 3-5 Microstructure of the microgel-stabilized emulsions. (i) The oil droplet surfaces of microgel-stabilized emulsions observed by cryo-SEM. (ii) CLSM images of the microgel-stabilized emulsions stained by Nile Blue A and Nile Red for agar-based ones, and ANS-Na and Nile Red for curdlan-based ones, respectively. The excitation and emission wave lengths of the dyes were 635 nm and 647 nm for Nile Blue A, 405 nm and 422 nm for ANS-Na, and 473 nm and 520 nm for Nile Red, respectively.

These results suggest that the particle size of microgels plays a critical role in successful creation of soybean oil-in-water emulsions stabilized by various polysaccharide microgels presumably because large particles adsorbed on the oil-water interface to form thick interfacial layers effectively preventing re-coalescence of created oil droplet surfaces during the emulsification processes. The successful emulsification observed above probably argues that agar and curdlan microgels adsorb to the oil-water interface as described for microgels prepared with other materials like inorganic polyacrylamide and edible proteins (Ngai et al., 2005; Destribats et al., 2014). In the following parts, the author investigated emulsion properties for

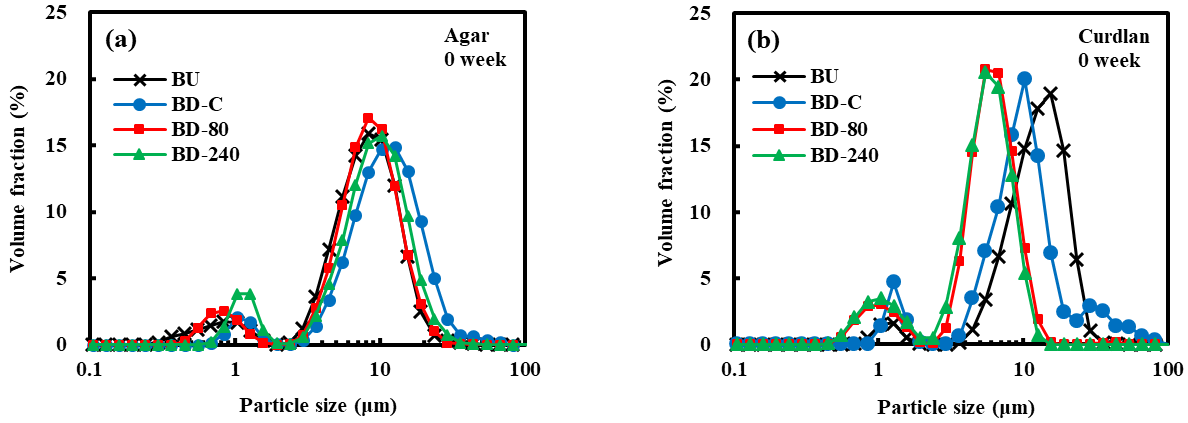

Fig. 3-6 Particle size distribution of the oil-in-water emulsions stabilized by microgels prepared with (a) agar and (b) curdlan. Measurements were carried out under the presence of SDS using a laser-diffraction particle size analyzer with a refractive index of 1.45 – 0.00*i* (n=3).

the agar and curdlan microgels.

To confirm the successful adsorption of microgel particles onto the oil droplet surfaces, the agar and curdlan microgel-stabilized emulsions were observed by cryo-SEM. Since similar images were obtained for BU, BD-80, and BD-240 emulsions made with agar and curdlan microgels, images of BD-240 and BD-C emulsions are presented in this section (Fig. 3-5 (i)). The oil droplet surfaces of agar BD-C and BD-240 emulsions seemed to be covered with the macromolecules, whereas those of the BD-C emulsions were slightly different from those of BD-240 ones (Fig. 3-5 (i-a) and (i-b)). The different structure cannot be necessarily attributed to the particle size of agar microgels as shown in Fig. 3-2. Compared to the oil droplet surfaces of agar microgel-based emulsions (Fig. 3-5 (i-a) and (i-b)) and curdlan BD-240 microgel-based emulsions (Fig. 3-5 (i-d)), those of curdlan BD-C microgel-based ones were likely surrounded by much larger microgel particles (Fig. 3-5 (i-c)). It is possible that only BD-C samples prepared via the formation of macrogels without ultra-high-pressure treatments

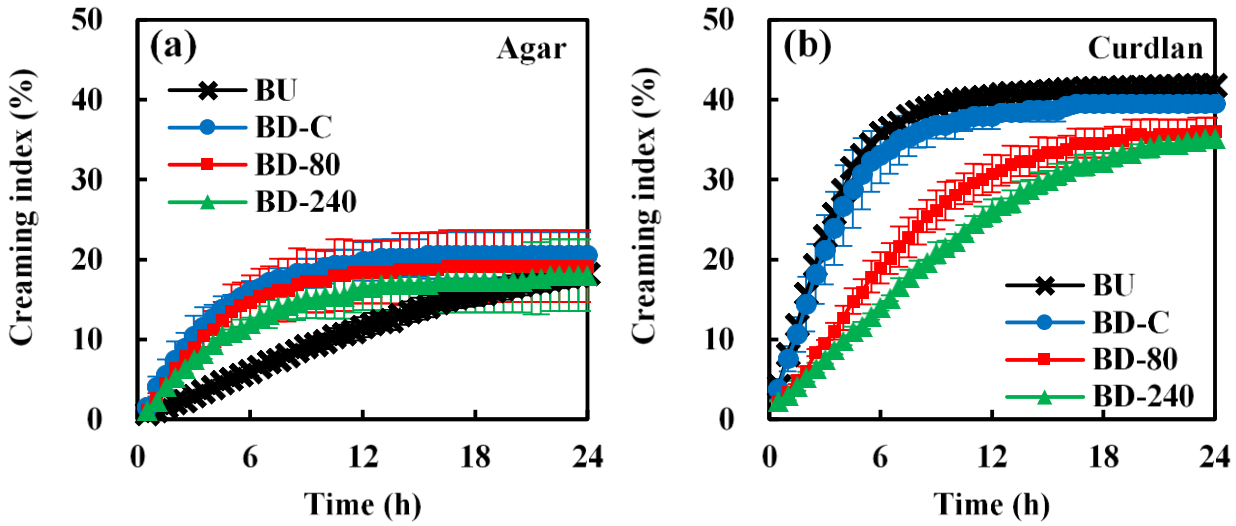

Fig. 3-7 Time-dependent change of creaming indices for the (a) agar and (b) curdlan microgel-stabilized emulsions (mean ± S.D., n=3). Experiments were carried out at 20°C for 24 h.

had such a unique structure.

The particle size distribution of the agar and curdlan microgel-stabilized emulsions was measured by a laser-diffraction particle size analyzer after diluting with deionized water including SDS that is helpful for excluding oil droplet aggregation and clarifying actual oil droplet size (Gelin et al., 1994). The oil droplet size distributions of all the samples did not significantly change regardless of the presence of SDS, indicating that the oil droplets did not strongly interact with each other to form aggregates under the tested conditions. Fig. 3-6 (a) presents the distributions of all the agar-based emulsion oil droplets prepared by the microgels fabricated via varied processing. They were generally all bimodal and the major peak was at around 10 μm. This tendency was observed for the curdlan-based emulsion oil droplets as well with a slight variation in the main peak (Fig. 3-6 (b)). The calculated mean value, $d_{4,3}$ of BU, BD-C, BD-80, and BD-240 emulsions was 6.07 ± 1.11, 8.27 ± 2.89, 7.21 ± 2.35, and 7.20 ± 2.03 μm for agar and 11.03 ± 2.50, 8.66 ± 1.03, 5.00 ± 0.47, and 4.61 ± 0.50 μm for curdlan,

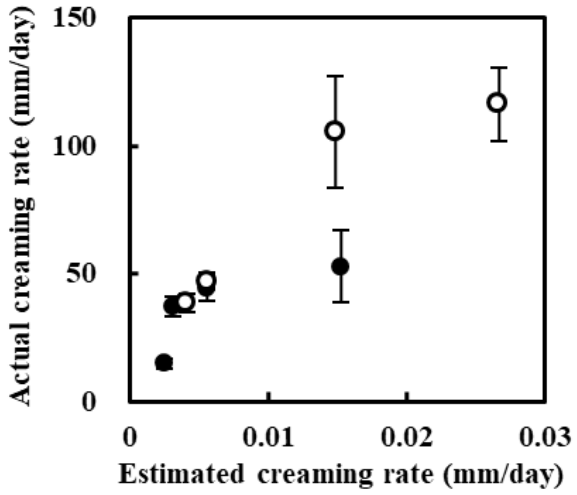

Fig. 3-8 Correlation of estimated and actual creaming rates of the microgel-stabilized emulsions. The estimation was performed based on the Stokes law using viscosity values of the corresponding continuous phases at the low shear rate (0.0096 s^{-1}) and the mean sizes of the emulsion oil droplets. The filled and open symbols indicate the values of agar- and curdlan-based emulsions, respectively.

respectively.

Emulsion stability

To evaluate emulsion stability against creaming, periodical macroscopic observations were carried out to calculate creaming index of the prepared emulsions. Fig. 3-7 (a) shows time-dependent changes of creaming index for the agar microgel-stabilized emulsions for 24 h static storage at 20°C. The creaming index of agar-based emulsions reached plateau after 24 h storage, but the creaming rate at the initial stage was much slower for BU samples than that for BD samples depending on the microgel preparation methods. On the contrary, reverse trends for the creaming rate with regard to the microgel processing were found as for curdlan-based emulsions (Fig. 3-7 (b)). The final creaming indices of agar and curdlan samples were of about 20% and 40%, respectively.

Based on the obtained results on $d_{4,3}$ of the emulsion oil droplets and viscosity of the continuous phase at the low shear rate shown above, the author calculated theoretical initial

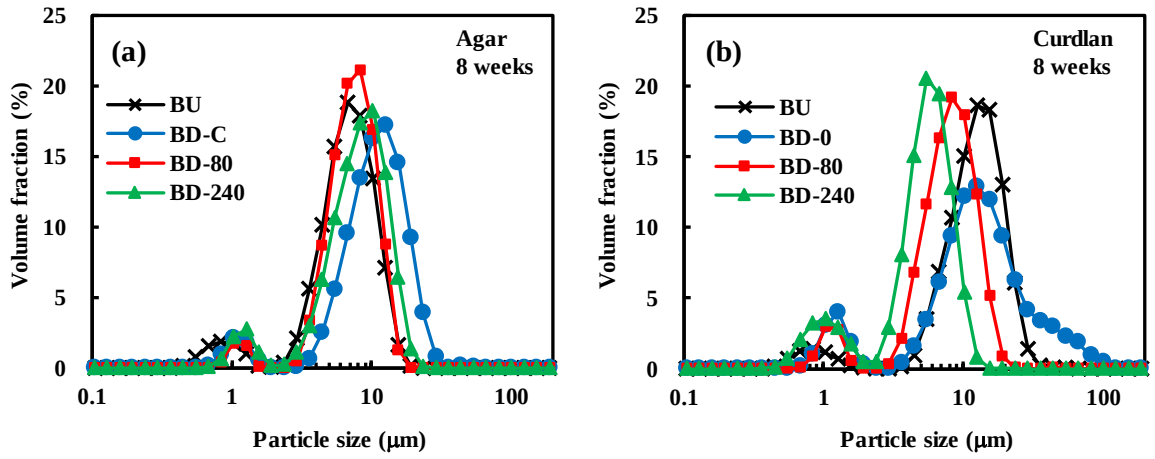

Fig. 3-9 Particle size distributions of the (a) agar microgel- and (b) curdlan microgel- based emulsions after 8 weeks storage at 25°C.

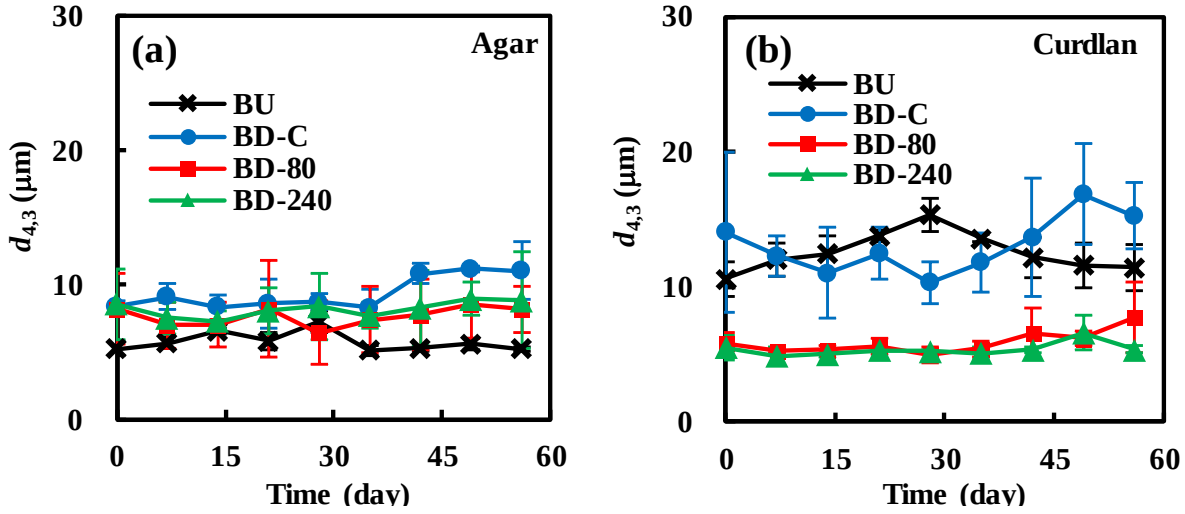

Fig. 3-10 Periodical change of $d_{4,3}$ of the (a) agar and (b) curdlan microgel-based emulsions measured using the particle size analyzer during storage test at 25°C.

creaming rate values of the samples using the Stokes law assuming that there are not any interactions between oil droplets which induce an increase of effective hydrodynamic radius of emulsion oil droplets. The used viscosity values of the BU, BD-C, BD-80, and BD-240 microgel dispersions were 54.6 ± 1.3, 16.8 ± 3.7, 34.3 ± 3.7, and 62.7 ± 34.5 Pa·s for agar and

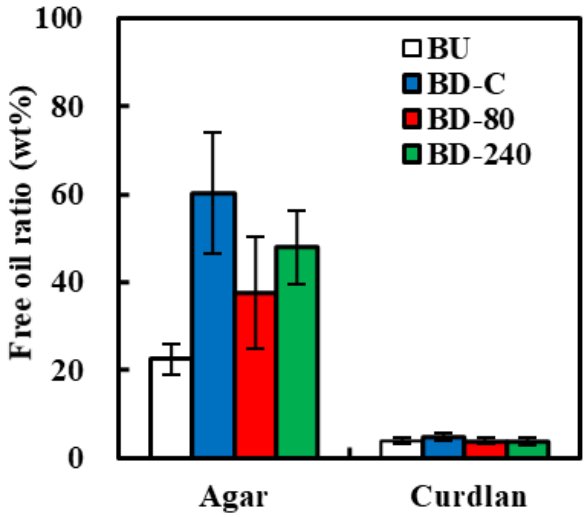

Fig. 3-11 Amount of free oils forcibly released from the microgel-based emulsions by centrifugation at 20,000×g for 30 min at 25°C.

17.2 ± 2.2, 18.9 ± 8.8, 16.7 ± 5.5, and 19.4 ± 8.2 Pa·s for curdlan, respectively (Fig. 3-4 (ii-a) and (ii-b)). Fig. 3-8 is a biplot graph of the observed initial creaming rates and the theoretical ones introduced by the Stokes law. The results show that the observed values were extremely higher than the theoretical values, demonstrating that the initial creaming rate of both agar and curdlan samples does not satisfy the assumption of the Stokes law, i.e., the emulsion oil droplets did considerably form flocculates that quickly cream, regardless of the high absolute values of zeta-potential of the emulsion oil droplets; that is, the values of BU, BD-C, BD-80, and BD-240 emulsions were -31.58 ± 5.71, -28.01 ± 2.93, -32.45 ± 1.43, and -34.83 ± 1.76 mV for agar and -32.38 ± 1.04, -35.93 ± 2.62, -37.23 ± 6.63, and -38.61 ± 7.79 mV for curdlan, respectively. This can be supported by microstructure of the microgel emulsions shown in Fig. 3-5 (ii). The molecular dynamics of microgels on the oil droplet surfaces and in the continuous phase such as overlapping etc. may have caused the significant flocculation.

As well as the initial creaming behavior, the final values of creaming index reached at the end of the measurements were clearly different between agar and curdlan samples (Fig. 3-7 (a) and (b)), suggesting that the packing states of the emulsion oil droplets were different between agar and curdlan samples. In order to clarify the existing state of oil droplets in the

continuous aqueous phase, microgel-based emulsions were prepared with fluorescence dyes to differentiate oil droplets and microgels by laser excitation in the CLSM observations (Fig. 3-5 (ii)). In general, the oil droplets of all the agar emulsions were packed less densely than those of all the curdlan emulsions, whilst the packing state seemed to be similar among the differently-treated microgel-based emulsions. The agar microgels appeared to be abundantly present among oil droplets to form a co-existing three-dimensional network, probably helpful for preventing the droplets from approaching each other that leads to no further creaming. Kaneda previously reported that agar microgel suspensions required small yield stresses to flow (Kaneda, 2006), indicating that such a network should exist in the agar microgel-based emulsions the author prepared.

To test emulsion stability against oil droplet coalescence during long-term static storage, time-dependent particle size measurements were performed by a laser diffraction particle size analyzer. Figs. 3-9 and 3-10 show the particle size distributions and the periodical change of volume-weighted mean particle diameter, $d_{4,3}$ of the samples. The particle size of all the emulsions did not considerably change for 8 weeks (Figs. 3-6, 3-9, and 3-10), obviously indicating that both the agar and curdlan microgel-based emulsions are extremely stable against oil droplet coalescence for long time under static conditions. The significantly high stability of the sample emulsions against coalescence was typically known for Pickering and Mickering emulsions and agrees with other previous reports (Destribats, 2014; Li, Li, Sun, & Yang, 2013). Meanwhile, the author measured the released free oils at the top after centrifugal acceleration of emulsion destabilization (Fig. 3-11). The amount of released oils from agar microgel-based emulsions was much larger than that from curdlan-based emulsions. This can be attributed to the different surface hydrophobicity that is related to the adsorption forces of microgels to the oil-water interface. That is, a more hydrophobic region of curdlan microgel particle surface is

able to penetrate oil droplets, more strongly anchoring microgel particles to oil droplets. Such strongly-bound microgels of curdlan may be resistant to the removal from oil droplets by the high speed centrifugation, thereby keeping thick layer to prevent coalescence.

In this study, the author investigated effects of microgelation on emulsifying ability of agar, curdlan, and gellan gum that have been scarcely utilized as stand-alone emulsifying agents. Agar and curdlan acquired the emulsifying ability via microgelation, whereas gellan gum did not. The averaged oil droplet size of the obtained agar and curdlan microgel stabilized emulsions was almost similar and totally independent of the preparation methods, i.e., build-up or break-down approaches. Among the major physical properties of microgel particles, the author can conclude that particle size of microgels particularly plays a critical role in stabilizing oil-in-water emulsions. The creaming stability of the obtained emulsions was significantly different depending on not only the kinds of polysaccharides but also the microgelation methods. All the emulsions were stable against oil droplet coalescence under the static condition, while the agar microgel-based emulsions destabilized under the accelerated dynamic condition, different from the curdlan microgel-based ones. The author is able to attribute the different behavior to the surface hydrophobicity of agar and curdlan microgles relating to solubilization of the fiber chains into the dispersed oil phases.

The surface hydrophobicity of agar and curdlan molecules is presumably originated from the carbon backbone and side chains with less polar groups of branched agar and the backbone of non-branched linear curdlan, in relation to the number of effective polar hydroxyl groups exposed to the water phase in an aqueous solution. Conversion of dispersed agar and curdlan polysaccharide molecules to microgels may have decreased the number of exposed hydroxyl groups throughout formation of intermolecular hydrogen bonding or molecular conformational changes due to the helices associations, that leads to the increased surface

hydrophobicity affecting the emulsion stability. Independent of the hydrophobicity, the author must again emphasize that emulsifying ability can be achieved by the micron-ordered microgels providing thick adsorbed layers on the oil droplet surfaces.

4. References

Armisén, R. & Galatas, F. Handbook of Hydrocolloids 2nd edn (eds Phillips, G. O. & Williams P. A.) Ch. 4 (Woodhead Publishing Limited, 2009).

Boral, S., & Bohidar, H. B. Effect of Ionic strength on surface-selective patch binding-induced phase separation and coacervation in similarly charged gelatin-agar molecular systems. *J. Phys. Chem. B* **114**,12027–12035 (2010).

Coviello, T., Matricardi, P., Marianecci, C., & Alhaique F. Polysaccharide hydrogels for modified release formulations. *J. Control. Release* **119**, 5–24 (2007).

Das, K. P. & Kinsella, J. E. Stability of food emulsions: physicochemical role of protein and nonprotein emulsifiers. *Adv. Food Nutr. Res.* **34**, 81–201 (1990).

Deshiikan, S. R. & Papadopoulos, K. D. London–vdW and EDL effects in the coalescence of oil drops. *J. Colloid Interface Sci.* **174**, 302–312 (1995).

Destribats, M., Rouvet, M., Gehin-Delval, C., Schmitt, C., & Binks, B. P. Emulsions stabilised by whey protein microgel particles: towards food-grade Pickering emulsions. *Soft Matter* **10**, 6941–6954 (2014).

Dickinson, E. Hydrocolloids at interfaces and the influence on the properties of dispersed systems. *Food Hydrocoll.* **17**, 25–39 (2003).

Dickinson, E. Microgels — An alternative colloidal ingredient for stabilization of food emulsions. *Trends Food Sci. Tech.* **43**, 178–188 (2015).

FAO & WHO Evaluation of allergenicity of genetically modified foods. *Report of a Joint FAO/WHO Expert Consultation on Allergenicity of Foods Derived from Biotechnology* (2001).

Fustier, P., Taherian, A. R., & Ramaswamy H.S. Functional Food Product Development (eds Smith, J. & Charter, E.) Ch. 4 (Blackwell Publishing Ltd, 2010)

Gelin, J. L., Poyen, L., Courthaudon, J. L., Le Meste, M., & Lorient, D. Structural changes in oil-in-water emulsions during the manufacture of ice cream. Food Hydrocoll. 8, 299–308 (1994).

Hefle, S. L., Nordlee, J. A., & Taylor, S. L. Allergenic foods. *Crit. Rev. Food Sci. Nutr.* **36** (Suppl), S69–S89 (1996).

Heo, S., Jeon, S., & Lee, S. Utilization of *Lentinus edodes* mushroom β-glucan to enhance the functional properties of gluten-free rice noodles. *LWT-Food Sci. Technol.* **55**, 627–631 (2014).

Hirano, I., Einaga, Y., & Fujita, H. Curdlan (bacterial b-1,3-glucan) in a cadoxen–water mixture. *Polym. J.*, **11**, 901–904 (1979).

Houben, A., Höchstötter, A., & Becker, T. Possibilities to increase the quality in gluten-free bread production: an overview. *Eur. Food Res. Technol.* **235**, 195–208 (2012).

Hunter, R. J. (ed) Foundations of Colloid Science 2nd edn (Oxford University Press, 2001).

Kaneda, I. The yield stress of a soft and water swellable microgel aqueous suspension in semi-dilute regime. *Nihon Reoroji Gakkaishi* (*J. Soc. Rheol., Jpn.*) **34**, 77–81 (2006).

Kato, A., & Nakai, S. Hydrophobicity determined by a fluorescence probe method and its correlation with surface properties of proteins. *Biochim. Biophys. Acta* **624**, 13–20 (1980).

Li, C., Li, Y., Sun, P., & Yang, C. Pickering emulsions stabilized by native starch granules. *Colloids Surf. A Physicochem. Eng. Asp.* **431**, 142–149 (2013).

Marti, A., & Pagani, M. A. What can play the role of gluten in gluten free pasta? *Trends Food Sci. Tech.* **31**, 63–71 (2013).

Matsumiya, K. & Murray, B. S. Soybean protein isolate gel particles as foaming and emulsifying agents. *Food Hydrocoll.* **60**, 206–215 (2016).

Matsumura, Y., Satake, C., Egami, M., & Mori, T. Interaction of gum arabic, maltodextrin and pullulan with lipids in emulsions. *Biosci. Biotechnol. Biochem*. **64**, 1827–1835 (2000).

McClements, D. J. (ed) Food Emulsions: principles, practices, and techniques 3rd edn (CRC Press, 2016).

Milas, M., Shi, X., & Rinaudo, M. On the Physicochemical Properties of Gellan Gum. *Biopolymers*, **30**, 451–464 (1990).

Mun, S., Cho, Y., Decker, E. A., & McClements, D. J. Utilization of polysaccharide coatings to improve freeze–thaw and freeze–dry stability of protein-coated lipid droplets. *J. Food Eng.* **86**, 508–518 (2008).

Murphy, R. W., Farkas, B. E., & Jones, O. G. Dynamic and viscoelastic interfacial behavior of β-lactoglobulin microgels of varying sizes at fluid interfaces. *J. Colloid Interface Sci*., **466**, 12–19 (2016).

Nakamura, A., Yoshida, R., Maeda, H., & Corredig, M. Soy soluble polysaccharide stabilization at oil–water interfaces. *Food Hydrocoll.* **20**, 277–283 (2006).

Ngai, T., Behrens, S. H., & Auweter H. Novel emulsions stabilized by pH and temperature sensitive microgels. *Chem. Commun.* **41**, 331–333 (2005).

Nishinari, K., Zhang, H., & Funami, T. Handbook of Hydrocolloids 2nd edn (eds Phillips, G. O. & Williams P. A.) Ch. 20 (Woodhead Publishing Limited, 2009).

Oh, J. K., Drumright, R., Siegwart, D. J., & Matyjaszewski, K. The development of microgels/nanogels for drug delivery applications. *Prog. Polym. Sci.* **33**, 448–477 (2008).

Palanuwech, J., Potineni R., Roberts, R. F., & Coupland, L. N. A method to determine free fat in emulsions. *Food Hydrocoll.* **17**, 55–62 (2003).

Pashley, R. M., Francis, M. J., & Rzechowicz, M. The hydrophobicity of non-aqueous liquids

and their dispersion in water under degassed conditions. *Curr. Opin. Colloid Interface Sci.* **13**, 236–244 (2008).

Pimentel, D. & Pimentel, M. Sustainability of meat-based and plant-based diets and the environment. *Am. J. Clin. Nutr.* **78** (Suppl), 660S–663S (2003).

Rabiey, L. & Britten, M. Effect of protein composition on the rheological properties of acid-induced whey protein gels. *Food Hydrocoll.* **23**, 983–979 (2009).

Rocha, C. M. R., Souza, H. K. S., Magalhães, N. F., Andrade, C. T., & Gonçalves, M. P. Rheological and structural characterization of agar/whey proteins insoluble complexes. *Carbohydr. Polym.* **110**, 345–353 (2014).

Schmidt, S, Liu, T., Rütten, S., Phan, K. H., Möller, M., & Richtering, W. Influence of microgel architecture and oil polarity on stabilization of emulsions by stimuli-sensitive core–Shell poly(*N*-isopropylacrylamide-co-methacrylic acid) microgels: Mickering versus Pickering behavior? *Langmuir* **27**, 9801–9806 (2011).

Seemann, S., Hauff, P., Schultze-Mosgau, M. Lehmann, C., & Reszka, R. Pharmaceutical evaluation of gas-filled microparticles as gene delivery system. *Pharm. Res.* **19**, 250–257, (2002).

Surh, J., Decker, E. A., & McClements, D. J. Influence of pH and pectin type on properties and stability of sodium-caseinate stabilized oil-in-water emulsions. *Food Hydrocoll.* **20**, 607–618 (2006).

Sworn, G. Handbook of Hydrocolloids 2nd edn (eds Phillips, G. O. & Williams P. A.) Ch. 9 (Woodhead Publishing Limited, 2009).

Takahashi R., Tokunou H., Kubota K., Ogawa E., Oida T., Kawase T., Nishinari K. Solution Properties of Gellan Gum: Change in Chain Stiffness between Single- and Double-Stranded Chains. *Biomacromolecules* **5**, 516–523 (2004).

Toufeili, I., Dagher, S., Shadarevian, S., Noureddine, A., Sarakbi, M., & Farran, M. T. Formulation of gluten-free pocket-type flat breads: optimization of methylcellulose, gum arabic, and egg albumen levels by response surface methodology. *Cereal Chem.* **71**, 594–601 (1994).

Tran, T. & Rousseau, D. Stabilization of acidic soy protein-based dispersions and emulsions by soy soluble polysaccharides. *Food Hydrocoll.* **30**, 382–392 (2013)

van Aken, G. A. Food Emulsions 4th edn (eds Friberg, S. E., Larsson, K., & Sjöblom, J.) Ch. 8 (Marcel Dekker, Inc, 2004).

Walstra, P. (ed) Physical Chemistry of Foods. (Marcel Dekker Inc., 2003).

Williams P. A. & Phillips, G. O. Handbook of Hydrocolloids 2nd edn (eds Phillips, G. O. & Williams P. A.) Ch. 1 (Woodhead Publishing Limited, 2009).

Wu, N. N., Huang, X., Yang, X. Q., Guo, J., Zheng, E. L., Yin, S. W., Zhu, J. H., Qi, J. R., He, X. T., & Zhang, J. B. Stabilization of soybean oil body emulsions using ι-carrageenan: Effects of salt, thermal treatment and freeze-thaw cycling. *Food Hydrocoll.* **28**, 110–120 (2012).

Yoshii, H., Soottitantawat, A., Liu, X. D., Atarashi, T., Furuta, T., Aishima, S., Ohgawara, M., & Linko, P. Flavor release from spray-dried maltodextrin/gum arabic or soy matrices as a function of storage relative humidity. *Innov. Food Sci. Emerg.* **2**, 55–61 (2001).

Zhang, Y., Wang, S., Zhou, J., Zhao, R., Benz, G., Tcheimou, J. S., Meredith, C., & Behrens, S. H. Interfacial activity of nonamphiphilic particles in fluid−fluid interfaces. Langmuir 33, 4511–4519 (2017).

Zhong, L., Fu, S., Peng, X., Zhan, H., & Sun, R. Colloidal stability of negatively charged cellulose nanocrystalline in aqueous systems. *Carbohydr. Polym.* **90**, 644–649 (2012).

SUMMARY

Chapter 1:

Interfacial and emulsifying properties of crude and purified soybean oil bodies

Soybean oil bodies are natural and environment-friendly emulsifying agents from plant resources required as a substitute for emulsifiers such as low-molecular-weight one and animal proteins. The aim of this study was to reveal the interfacial properties and the emulsifying properties of two types of oil bodies extracted from soybean seeds at different pH conditions, that is purified oil bodies (OB) and crude oil bodies (OBC) including storage and other minor proteins. Particle size and zeta-potential measurements and SDS-PAGE revealed that the presence of the involved storage and other minor proteins promoted oil body aggregations and imparted the high zeta-potential to the oil bodies. OB adsorbed onto the oil-water (O/W) interface in closely packed state and formed more elastic adsorbed layer than OBC according to the results from tensiometry. Emulsions stabilized by OB (OB-E) were more stable against oil droplet coalescence than those by OBC (OBC-E) due to the absence of the involved proteins at the emulsion droplet surfaces. Cryo-SEM observation suggests that during emulsification most of the OB and OBC particles adsorbed onto the newly-created O/W interface and then rapidly ruptured.

Chapter 2:

Effects of acid and salt addition on the colloidal and emulsifying properties of soybean oil bodies

Soybean oil bodies (OBs) are natural molecular-assemblies containing lipophilic components. This study clarifies the effects of acid and salt addition on the interfacial and emulsifying properties of OBs. Extracted OBs were dispersed to 10 mM sodium acetate buffer solutions (pH 4.0 – 5.5) containing 0, 50, or 100 mM sodium chloride. Colloidal, interfacial, and emulsifying properties of OBs were analyzed. The zeta-potential of OBs lowered as the pH value and salt concentration increased. The particle size analysis revealed that OBs were submicron particles and tend to aggregate at pH 5.0 and 5.5 under low salt conditions probably due to the weak electrostatic repulsion. The interfacial tension at the oil-water interface rapidly decreased by OB adsorption under the weakly acidic conditions especially (pH 5.0 and 5.5), suggesting that the lowered zeta-potential contributes to the higher amount of OB adsorption via the formation of large aggregated-OB enabling the efficient coverage and/or the reduction of electrostatic barrier caused by adsorbed and unadsorbed OBs. OBs formed elastic films at the oil-water interfaces. The formation of viscoelastic films at the oil-water interfaces is responsible for high coalescence stability of OB-stabilized emulsions for long-term storage.

Chapter 3:

Microgelation imparts emulsifying ability to surface-inactive polysaccharides—bottom-up vs top-down approaches

In order to impart emulsifying ability to gel-forming polysaccharides that have not been used as emulsifying agents, three kinds of polysaccharides, agar, curdlan, and gellan gum were converted to microgels by different gelation methods via the bottom-up and top-down approaches. The author clearly demonstrated that agar and curdlan acquired the ability to emulsify an edible oil by microgel formation. Among the colloidal properties of microgel

suspensions such as microstructure, particle size, zeta-potential, viscosity, and surface hydrophobicity, The author pointed out the importance of particle size on the emulsifying ability of polysaccharide-based microgels. The creaming behavior of the microgel-stabilized emulsions depended on the polysaccharide types and microgel preparation methods. The emulsion stability against oil droplet coalescence was extremely high for agar and curdlan microgel-stabilized emulsions during storage in the static condition, whereas different stability was observed for both the emulsions, that is, the curdlan microgel-based ones were more resistant to dynamic forcible destabilization by centrifugation than the agar ones, which can be attributed to the surface hydrophobicity of the microgels.

ACKNOWLEDGEMENTS

First of all, the author would like to express the deepest respect and gratitude to Dr. Yasuki Matsumura, Professor of Laboratory of Quality Analysis and Assessment, Graduate School of Agriculture, Kyoto University for his kind guidance, invaluable discussion, and heartfelt encouragements throughout this study.

The author is greatly indebted to Dr. Yukako Hayashi, Associate Professor of Laboratory of Quality Analysis and Assessment, Graduate School of Agriculture, Kyoto University for her suggestive comments and continuous encouragements.

The author would like to express his sincere appreciate to Dr. Kentaro Matsumiya, Assistant Professor of Laboratory of Quality Analysis and Assessment, Graduate School of Agriculture, Kyoto University for his heartfelt instructions, insightful advices, and continuous supports.

The author would greatly appreciate to Ms. Yuko Nambu and Ms. Mai Aoshima for their great support during the experiments.

The author must acknowledge to Dr. Samoto Masahiko and Dr. Takenobu Ogawa for insightful discussion with them.

I would like to offer my special thanks to Mr. Hiroshi Murakami for his warmful support since I was an undergraduate student.

Acknowledgement is also extended to Ms. Sachie Kimoto for her daily support and heart-warming attitude during the graduate study.

The author thank many colleagues, including Ms. Jiraporn Sirison, Ms. Rio Sasabe, Ms. Mio Sasaki, Ms. Mika Horii, Mr. Ryo Yoshida, Ms. Yoko Sakurai, Mr. Akira Trii, Mr. Yasuhiro Dohguchi, Ms. Mai Utsumi, Mr. Koki Kato, Ms. Kaho Kanatani, Ms. Yurie

Takei, Mr. Kenji Okumura, Ms. Rihoko Shimizu, Mr. Fujimoto, Ms. Hsin-Hsuan Ho, Ms. Ai Sato, Ms. Miki Tatsumi, Ms. Sakuko Ichinomiya, Mr. Atsushi Dan, Mr. Satoshi Yamashita, Mr. Kohei Yokota, Ms. Sayaka Fujiki, and Ms. Ayane Shigemoto for their helpful advices and encouragement during my study.

Finally, the author is deeply indebted to his family for their warmful supports and love during the long years of the graduate study in Kyoto University.

LIST OF PUBLICATION

1. Interfacial and emulsifying properties of crude and purified soybean oil bodies.

   Toya Ishii, Kentaro Matsumiya, Yuko Nambu, Masahiko Samoto, Masanobu Yanagisawa, & Yasuki Matsumura, Food Structure, 12, 64–72 (2017)

   DOI: 10.1016/j.foostr.2016.12.005

2. Microgelation imparts emulsifying ability to surface-inactive polysaccharides—bottom-up vs top-down approaches.

   Toya Ishii, Kentaro Matsumiya, Mai Aoshima, & Yasuki Matsumura, npj Science of Food, 2, 15 (2018)

   DOI: 10.1038/s41538-018-0023-7